# ~~The relaxation~~Post-entrapment modification of residual inclusion pressure and its implications to Raman~~-~~ elastic thermobarometry

Xin Zhong[*1]; Evangelos Moulas[2]; Lucie Tajčmanová[3]

1 Physics of Geological Processes, The Njord Center, University of Oslo, Oslo, Norway

~~2 Institut des sciences de la Terre, Université de Lausanne, Lausanne, Switzerland~~

2 Institute of Geosciences, Johannes Gutenberg University Mainz, Mainz, Germany

3 Institute of Earth Sciences, Heidelberg University, Heidelberg, Germany

Correspondence to: Xin Zhong (xinzhong0708@gmail.com)

**Abstract:** Residual pressure can be preserved in mineral inclusions, e.g. quartz-in-garnet, after exhumation due to differential expansion between inclusion and host crystals. Raman spectroscopy has been applied to infer the residual pressure and provides information on the entrapment temperature and pressure conditions. However, the amount of residual pressure relaxation cannot be directly measured. An underestimation/overestimation of residual pressure ~~relaxation~~ may lead to significant errors between calculated and actual entrapment pressure. This study focuses on three mechanisms responsible for the residual-pressure ~~relaxation~~modification: 1) viscous creep; 2) plastic yield; 3) proximity of inclusion to thin-section surface. Criteria are provided to quantify how much of the expected residual pressure is ~~relaxed~~modified due to these three mechanisms. An analytical solution is introduced to demonstrate the effect of inclusion depth on the residual pressure field when the inclusion is close to thin-section surface. It is shown that for quartz-in-garnet system, the distance between thin-section surface and inclusion centre needs to be at least ~~two~~three times the inclusion radius to avoid pressure ~~relaxation~~release. In terms of viscous creep, representative case studies on quartz-in-garnet system show that viscous relaxation may occur from temperatures as low as 600~700 ℃ depending on the particular pressure-temperature (*P-T*) path and various garnet compositions. For quartz entrapped along the prograde *P-T* path and subject to viscous ~~resetting~~relaxation at peak *T* above 600~700 ℃, its residual

pressure after exhumation may be higher than predicted from its true entrapment conditions. Moreover, such a viscous resetting effect may introduce apparent overstepping of garnet nucleation that is not related to reaction affinity.

## 1. Introduction

During metamorphism, the growth of porphyroblasts often results in the entrapment of ~~inclusions, e.g. quartz inclusion entrapped in garnet host.~~solid/fluid inclusions, which then provide important information about the rock's history (e.g. Farber et al., 2014; Yardley and Bodnar, 2014; Ferrero and Angel, 2018). Due to the differences in the elastic compressibility and thermal expansion coefficient between the inclusion and host, residual inclusion pressures may be preserved after exhumation (e.g. Rosenfeld and Chase, 1961; Gillet et al., 1984; Zhang, 1998; Angel et al., 2015). The residual pressure can be inferred by Raman shift based on experimental calibrations, e.g. quartz inclusions (e.g. Liu and Mernagh, 1992; Schmidt and Ziemann, 2000). This allows the application of Raman-thermobarometry to infer the entrapment pressure and temperature (*P*-*T*) conditions ~~(e.g. Ashley et al., 2014; Bayet et al., 2018; Enami et al., 2007; Izraeli et al., 1999; Kohn, 2014; Spear et al., 2014; Taguchi et al., 2019; Zhong et al., 2019)~~(e.g. Ashley et al., 2014; Bayet et al., 2018; Enami et al., 2007; Izraeli et al., 1999; Kohn, 2014; Spear et al., 2014; Taguchi et al., 2019; Zhong et al., 2019). Existing models that link residual pressure and entrapment *P*-*T* conditions are based on elastic rheology and often assume infinite host radius ~~(e.g. Rosenfeld and Chase, 1961; Van Der Molen and Van Roermund, 1986; Guiraud and Powell, 2006; Angel et al., 2017). Recent~~(Rosenfeld and Chase, 1961; Van Der Molen and Van Roermund, 1986; Guiraud and Powell, 2006; Angel et al., 2017b). Despite these simplifications, recent experimental works have been successfully performed to compare the measured residual pressure with modelled residual pressure under well-controlled *P*-*T* conditions for synthetic samples with quartz-in garnet system (Thomas and Spear, 2018; Bonazzi et al., 2019).

Although many studies using Raman spectroscopy reported maximal residual pressure close to the predictions from elastic model (e.g. Ashley et al., 2014; Enami et al., 2007; Zhong et al., 2019), a large amount of inclusion pressure estimates are lower than theoretically predicted by the elastic model (Korsakov et al., 2009; Kouketsu et al., 2016; Yamamoto et al., 2002). The ~~relaxation~~modification of inclusion pressure can be due to various reasons and a systematic investigation is critical to better apply Raman-thermobarometry to natural samples. Meanwhile, Raman-thermobarometry has been employed to

investigate the amount of overstepping for garnet growth by comparing the *P-T* constraints from phase equilibria and elastic thermobarometry ~~(Spear et al., 2014; Wolfe and Spear, 2017). The relaxation of residual inclusion pressure may lead to errors in the calculated reaction affinities (e.g. Castro and Spear, 2017).~~(Spear et al., 2014; Castro and Spear, 2017; Wolfe and Spear, 2017). Particularly, when comparing the determined paleopressures based on phase equilibria and elastic barometry using quartz-in-garnet system, careful examination on the amount of residual quartz pressure modification due to the creep of garnet host becomes critical.

When a mineral inclusion maintains residual pressure, differential stress is concomitantly developed around the inclusion on the host side to maintain mechanical equilibrium (e.g. Zhang, 1998; Tajčmanová et al., 2014). The host mineral may experience viscous creep which is manifested by the dislocation structures ~~(Chen et al., 1996; Yamamoto et al., 2002). Furthermore, the host mineral may also form radial/tangential (micro) cracks due to plastic yield when the differential stress exceeds the yield criterion (Van Der Molen and Van Roermund, 1986; Whitney, 1991).~~(Chen et al., 1996; Yamamoto et al., 2002; Taguchi et al., 2019b). Furthermore, the host mineral may also experience rate-independent plastic yield when the differential stress exceeds the yield criterion (e.g. Zhang, 1998). In the mechanics literature, plastic deformation is commonly considered as any inelastic deformation (time-dependent and time-independent) (e.g. Kachanov, 1971). In this work, we distinguish between viscous creep, i.e. the rate-dependent inelastic deformation and the rate-independent plastic flow. Mechanical models show that both viscous creep (dislocation or diffusion creep of host) and plastic ~~yield (radial or tangential micro-cracks)~~flow during decompression and cooling can cause significant inclusion pressure ~~relaxation~~drop (Dabrowski et al., 2015; Zhang, 1998). This would lead to an underestimate of residual inclusion pressure (Zhong et al., 2018b) (Fig. 1). Meanwhile, during the thin-section preparation, mineral inclusions are positioned into proximity towards the thin-section surface (Fig. 1). The thin-section surface is stress free and may elastically ~~relax~~release the residual pressure (Mindlin and Cheng, 1950; Seo and Mura, 1979; Zhong et al., 2018a). It is of petrological interest to study how deep the inclusion needs to be in order to preserve the residual pressure. Experimental works and numerical simulations with finite element method have been performed to test the safe inclusion depth (inclusion radius less than one ~~half~~third of host radius) so that the residual inclusion pressure can be preserved for the application of Raman barometry (Campomenosi et al., 2018; Mazzucchelli et al., 2018).

In this contribution, we systematically investigate the following mechanisms for residual inclusion pressure ~~relaxation~~modification: 1) viscous creep of the host materials ~~that causes viscous relaxation of residual pressure~~, 2) plastic yield ~~that causes (micro)-cracks that relax~~within the ~~residual pressure~~host, and 3) ~~relaxation~~pressure release due to the proximity of inclusion towards thin-section surface. For the first and second purposes, a 1D visco-elasto-plastic mechanical model is developed in radially symmetric spherical coordinate frame ~~to study the effect of viscous relaxation and plastic yield of the residual entrapment pressure.~~ The derived system of equations is nondimensionalized to extract the key parameters that control the amount of viscous relaxation and plastic yield ~~of the residual pressure.~~ For the third ~~purpose, an~~mechanism, a simple analytical solution for the ~~entrapment~~residual inclusion pressure field close to thin-section surface is introduced ~~as a simplified form~~ based on the existing work of Seo and Mura (1979). The analytical solution demonstrates the effect of the inclusion depth that controls the amount of pressure ~~relaxation~~release. This solution applies to the case where the inclusion possesses the same elastic moduli as the host~~, and the stress is generated due to the differential thermal expansion/contraction.~~. The inclusion is initially subject to an arbitrary hydrostatic pressure in infinite host and its pressure is released as it moved towards a stress-free thin-section surface. In comparison, for natural quartz-in-garnet system, numerical solutions are applied to investigate the safe distance that causes negligible pressure ~~relaxation~~release due to the presence of thin-section surface~~.~~ (stress-free boundary). In this study, both inclusion and host are treated as elastically isotropic as an assumption to put focus on the effect of these three mechanisms on preserved residual pressure. The effects of elastic anisotropy for commonly encountered quartz inclusion have been studied experimentally and theoretically by e.g. Murri et al. (2018) and Campomenosi et al. (2018) and are discussed in the end.

## 2. ~~Methods~~1D mechanical model with visco-elasto-plastic rheology

### ~~2.1 Visco-elasto-plastic mechanical model~~

~~To investigate the effect of viscous creep and plastic yield on residual pressure, we~~2.1 Governing equations

We develop a 1D mechanical model with spherical symmetry that is based on the conservation of mass and momentum~~, and it employs a Maxwell visco-elasto-plastic rheology.~~. In 1D radially symmetric spherical coordinate frame, mechanical equilibrium is expressed as follows:

$$\frac{\partial \tau_{rr}}{\partial r} + \frac{3\tau_{rr}}{r} - \frac{\partial P}{\partial r} = 0, \quad (1)$$

where $\tau_{rr}$ is the radial component of deviatoric stress ($Pa$), $P$ is pressure ($Pa$) and $r$ is radial coordinate ($m$). We apply the Maxwell visco-elasto-plastic rheology ~~to express stress-strain (rate) relation in the radial direction~~ as follows:

~~$$\dot{e}_{rr} = \underbrace{\frac{\dot{\tau}_{rr}}{2G}}_{elastic} + \underbrace{\frac{\tau_{rr}}{2\eta}}_{viscous} + \underbrace{\lambda\, sign(\tau_{rr})}_{plastic},$$~~ $\dot{e}_{rr} = \dot{e}^{e}_{rr} + \dot{e}^{v}_{rr} + \dot{e}^{p}_{rr}$, (2)

~~where the dot above $\dot{\tau}_{rr}$ denotes time derivative, $\dot{e}_{rr}$ is the radial component of the deviatoric strain rate ($s^{-1}$) that is composed of elastic, viscous and plastic counterparts, $G$ is shear modulus ($Pa$), $\eta$ is viscosity ($Pa \cdot s$), $\lambda$ is the plastic multiplier ($s^{-1}$) which guarantees that the plastic yield criterion is not exceeded.~~where $\dot{e}_{rr}$ is the radial components of the deviatoric strain rate ($s^{-1}$) composed of elastic, viscous (rate-dependent) and plastic (rate-independent) parts. The elastic and viscous strain rates are expressed as:

$$\dot{e}^{e}_{rr} = \frac{\dot{\tau}_{rr}}{2G}, \quad (3)$$

$$\dot{e}^{v}_{rr} = \frac{\tau_{rr}}{2\eta},$$

where the dot above $\dot{\tau}_{rr}$ denotes time derivative, $G$ is shear modulus ($Pa$), $\eta$ is viscosity ($Pa \cdot s$). The non-Newtonian (effective) viscosity is expressed as follows:

~~The plastic strain rate is obtained by using the Tresca yield criterion (see e.g. Ranalli, 1995):~~

~~$F = |\tau_{rr} - \tau_{tt}| - C, \eta = A|\tau_{rr}|^{1-n}$,~~ (~~43~~)

where ~~$C$ is plastic cohesion ($Pa$) that controls the occurrences of (micro) cracks, and $\tau_{tt}$ is the tangential component of deviatoric stress. Due to spherical symmetry, we also~~where $A$ is the temperature dependent pre-factor and $n$ is the stress exponent (e.g. Dabrowski et al. 2015, eq. 10). The plastic strain rate is obtained by using the Tresca yield criterion (e.g. Kachanov, 1971):

$$F = |\tau_{rr} - \tau_{tt}| - C, \quad (5)$$

where $C$ is plastic yield strength ($Pa$), and $\tau_{tt}$ is the tangential component of deviatoric stress. Due to spherical symmetry, we have $\tau_{tt} = -1/2\tau_{rr}$. Applying the plastic flow law (e.g. Vermeer and De Borst, 1984), we get:

$$\dot{e}^p_{rr} = \lambda \frac{\partial F}{\partial \tau_{rr}} = \lambda \, ~~sign(\tau_{rr}),~~ sgn(\tau_{rr}) = \lambda\delta, \begin{cases} \lambda = 0 \text{ for } F \leq 0 \\ \lambda \neq 0 \text{ for } F > 0 \end{cases} \quad (~~64~~)$$

where $\lambda$ is the plastic multiplier ($s^{-1}$), which provides the amount of plastic strain (rate) that guarantees the yield criterion is not exceeded, and $\delta$ is the sign of $\tau_{rr}$. For isotropic materials, the pressure (negative mean stress)~~The non-Newtonian (effective) viscosity is expressed as follows:~~

~~$\eta = A|\tau_{rr}|^{1-n}$,~~ ~~(5)~~

~~where $A$ is the temperature dependent pre-factor for viscosity ($Pa^n \cdot s$), $n$ is the stress (power law) exponent. The pressure~~ can be expressed as a function of volume and temperature via equation of state (EoS), and its time derivative is as follows:

$$\dot{P} = -\dot{\varepsilon}_{kk}/\beta + \alpha\dot{T}/\beta, \quad (~~76~~)$$

where $\beta$ is compressibility ($1/Pa$), $\alpha$ is the thermal expansion coefficient ($1/K$), $\dot{T}$ is the rate of temperature change ($K/s$). Temperature is treated as homogeneous within inclusion-host system. Einstein summation is used here for the volumetric strain rate ($\dot{\varepsilon}_{kk} = \dot{\varepsilon}_{rr} + 2\dot{\varepsilon}_{tt}$~~).~~, where due to spherical symmetry the two tangential strain rates are equal). No viscous or plastic volumetric strain is considered. This assumption is a good approximation for non-porous, crystalline materials (e.g. Moulas et al., 2019).

~~By~~Substituting Eq. 3 and Eq. 6 into Eq. 2 and applying first-order finite difference in time to Eq. 2 and Eq. ~~7~~6 (i.e. $\dot{\tau}_{rr} = \frac{\tau_{rr}-\tau_{rr}^o}{\Delta t}$ and $\dot{P} = \frac{P-P^o}{\Delta t}$), we can explicitly express $\tau_{rr}$ and $P$ as:

$$\tau_{rr} = 2\eta Z\dot{e}_{rr} + (1-Z)\tau_{rr}^o ~~- 2\eta Z\lambda\, sign(\tau_{rr}),~~ - 2\eta Z\lambda\delta, \quad (~~8~~7)$$

$$P = P^o - \Delta t\dot{\varepsilon}_{kk}/\beta + \alpha\,\triangle\, t\dot{T}/\beta, \quad (~~9~~8)$$

where $Z = \frac{~~\Delta tG~~}{~~\Delta tG+\eta~~}\frac{\Delta tG}{\Delta tG+\eta}$ is the viscoelastic coefficient, $\tau_{rr}^o$ is the radial component of deviatoric stress in the previous time step, $P^o$ is the pressure in previous time step. If the yield criterion in Eq. ~~5~~3 is exceeded ($F > 0$), the plastic multiplier must be ~~correctly chosen~~adjusted to drive $F$ to zero. This can be achieved by substituting the deviatoric stress (Eq. ~~8~~7) into Eq. ~~5~~3 and let $F = 0$. Therefore, we obtain $\lambda$ as follows:

$$\lambda = \delta\dot{e}_{rr} + ~~\frac{(1-Z)sign(\tau_{rr})}{2\eta Z}\tau_{rr}^o~~ - ~~\frac{C}{3\eta Z}~~\frac{(1-Z)\delta}{2\eta Z}\tau_{rr}^o - \frac{\delta C}{3\eta Z}, \quad \text{if } F > 0 \text{ (otherwise } \lambda = 0). \quad (~~10~~9)$$

### 2.2 Nondimensionalization

The variables in the above equations can be scaled to derive nondimensional parameters for better understanding the behaviour of the inclusion-host system. This is done by choosing the following ~~independent scales:~~six parameters to nondimensionalize the system of equations: the temperature drop of the host-inclusion system $\Delta T$, the inclusion radius $R$, ~~temperature change $\Delta T$,~~ the time of the $P-T$ path $t^*$, the host's viscosity pre-factor ~~$A_h$ of~~$A_{\mathrm{h}}$, the host~~,~~'s plastic ~~cohesion~~yield strength ~~$C_h$ of host,~~$C_{\mathrm{h}}$, and the expected pressure perturbation $P_{~~exp~~\mathrm{exp}}$ that is given as follows:

$$~~P_{exp} = \frac{\Delta P(\beta_i-\beta_h)-\Delta T(\alpha_i-\alpha_h)}{\beta_i+3/4G_h},~~ P_{\mathrm{exp}} = \frac{\Delta P(\beta_i-\beta_h)-\Delta T(\alpha_i-\alpha_h)}{\beta_i+3/4G_h}, \quad (11~~10~~)$$

~~where $\Delta P, \Delta T$ are the confining pressure and temperature drops from entrapment to the Earth's surface, $\beta_i$ and $\beta_h$ are the compressibility of inclusion and host, $\alpha_i$ and$\alpha_h$ are the thermal expansion coefficients of inclusion and host, $G_h$ is the shear modulus of host.~~

~~By choosing $P_{exp}$ as the scale, residual pressure will vary around zero to one. This pressure scale allows convenient quantification for viscous and plastic relaxation.~~

~~The involved physical variables are scaled as shown below:~~

where $\Delta P, \Delta T$ are the confining pressure and temperature drops from entrapment to the Earth's surface, $\beta_i$ and $\beta_h$ are the compressibility of inclusion and host, $\alpha_i$ and $\alpha_h$ are the thermal expansion coefficients of inclusion and host, $G_h$ is the shear modulus of host. The number $P_{\text{exp}}$ is the expected amount of residual inclusion pressure after exhumation assuming linear thermo-elasticity and infinite host (Zhang, 1998). It is noted that this is not the actual final residual inclusion pressure, but merely a scale to nondimensionalize the stress (and pressure). By choosing $P_{\text{exp}}$ as the stress scale, the inclusion residual pressure is expected to be between 0 and 1 for a case of cooling and decompression. This pressure scale allows convenient quantification for the amount of pressure modification due to viscous creep and plastic yield. The involved physical variables are scaled as shown below:

$$r = R\,\bar{r}$$

$$\beta = \frac{1}{P_{exp}}\frac{1}{P_{\text{exp}}}\bar{\beta}$$

$$G = P_{exp}P_{\text{exp}}\bar{G}$$

$$\alpha = \frac{1}{\Delta T}\bar{\alpha}$$

$$P = P_{exp}P_{\text{exp}}\bar{P}$$

$$\dot{T} = \frac{\Delta T}{t^*} = \frac{\Delta T}{t^*}\bar{\dot{T}} \qquad (12\text{~~11~~})$$

$$\tau_{rr} = P_{exp}P_{\text{exp}}\overline{\tau_{rr}}$$

$$C = C_h C_{\text{h}}\bar{C}$$

$$\eta = P_{exp}P_{\text{exp}}t^*\bar{\eta}$$

$$F = P_{exp}C_{\text{h}}\bar{F}$$

$$\Delta t = t^*\overline{\Delta t}$$

$$A = \sout{A_h} A_{\mathrm{h}} \bar{A}$$

$$\lambda = \frac{1}{t^*}\bar{\lambda}$$

$$v_r = \frac{R}{t^*}\overline{v_r}$$

where the overhead bars indicate dimensionless properties. Substituting these scaling equations into Eq. 1, 8~~7~~ and 9~~8~~, we get:

$$\frac{\partial \overline{\tau_{rr}}}{\partial \bar{r}} + \frac{3\overline{\tau_{rr}}}{\bar{r}} - \frac{\partial \bar{P}}{\partial \bar{r}} = 0, \tag{13~~12~~}$$

$$\bar{P} = \overline{P^o} + \frac{1}{\bar{\beta}}\sout{\left[-\overline{\Delta t}\frac{\partial \bar{r}^2 \overline{v_r}}{\bar{r}^2 \partial \bar{r}} + \bar{\alpha}\bar{T}\right]}\left[-\overline{\Delta t}\frac{\partial \bar{r}^2 \overline{v_r}}{\bar{r}^2 \partial \bar{r}} + \bar{\alpha}\bar{T}\right], \tag{14~~13~~}$$

$$\overline{\tau_{rr}} = \frac{4}{3}\bar{\eta}\bar{Z}\left(\frac{\partial \overline{v_r}}{\partial \bar{r}} - \frac{\overline{v_r}}{\bar{r}}\right) + (1-\bar{Z})\overline{\tau_{rr}^o} - 2\bar{\eta}\bar{\lambda}\delta\bar{Z}, \tag{15~~14~~}$$

where dimensionless viscosity, viscoelastic coefficient and plastic multiplier are expressed as:

$$\bar{\eta} = De \cdot \overline{A|\tau_{rr}|}^{1-n}, \tag{16~~15~~}$$

$$\bar{Z} = \sout{\frac{\overline{\Delta t}\bar{G}}{\overline{\Delta t}\bar{G}+\bar{\eta}}} = \frac{\overline{\Delta t}\bar{G}}{\overline{\Delta t}\bar{G}+\bar{\eta}}, \tag{17~~16~~}$$

$$\bar{\lambda} = \frac{4}{3}\delta\left(\frac{\partial \overline{v_r}}{\partial \bar{r}} - \frac{\overline{v_r}}{\bar{r}}\right) + \frac{(1-\bar{Z})\delta}{2\bar{\eta}\bar{Z}}\overline{\tau_{rr}^o} - C^* \cdot \sout{\frac{\bar{C}}{3\bar{\eta}\bar{Z}}}\frac{\bar{C}}{3\bar{\eta}\bar{Z}}, \text{ if } \sout{\frac{3}{2}\delta\overline{\tau_{rr}} - C^* \cdot \bar{C}\bar{F} > 0.} \tag{18~~17~~}$$

Two dominant dimensionless numbers emerge after nondimensionalization. They are Deborah number $De$ and ~~Cohesion number~~dimensionless yield strength $C^*$ defined as follows:

$$De = \sout{\frac{A_h/P_{exp}^n}{t^*}}\frac{A_{\mathrm{h}}/P_{\mathrm{exp}}^n}{t^*}, \tag{19~~18~~}$$

$$C^* = \sout{\frac{C_h}{P_{exp}}}\frac{C_{\mathrm{h}}}{P_{\mathrm{exp}}}. \tag{20~~19~~}$$

~~where $A_h$ is the pre-factor of viscosity of the host, $n$ is stress exponent, $t^*$ is the duration of viscous relaxation, $C_h$ is the cohesion of host.~~

~~The Deborah number ($De$) is the ratio between the characteristic viscous relaxation time ($A_{\text{n}}/P_{exp}^{n}$) and model duration ($t^*$).~~The Deborah number ($De$) is the ratio between the characteristic viscous relaxation time ($A_{\text{h}}/P_{\text{exp}}^{n}$) and model duration ($t^*$) (Reiner, 1964). If $De > 1$, the system behaves in an elastic manner, and if $De < 1$, viscous creep becomes important. The pre-factor of viscosity is temperature dependent. By choosing the pre-factor ~~$A_{\text{n}}$~~$A_{\text{h}}$ at peak temperature, one can directly use $De$ to estimate the maximal amount of viscous relaxation. This is especially suitable for the process of isothermal decompression in many high-pressure rocks.

The ~~Cohesion number~~dimensionless yield strength $C^*$ characterizes the ability of a host mineral to plastically yield and a high ~~Cohesion number~~$C^*$ implies that the material is less prone to plastic yield~~.~~ given the amount of residual inclusion pressure $P_{\text{exp}}$. The viscosity of different mineral phases may vary by orders of magnitude, and the ~~cohesion of difference mineral~~plastic yield strength of different minerals may also vary by ~~many~~ several factors~~, potentially orders of magnitude~~. Therefore, these two dimensionless numbers have a dominant effect on the amount of inclusion pressure modification due to viscous relaxation and plastic yield.

### 2.3 Numerical approach for visco-elasto-plastic model

The dimensionless viscosity (Eq. 16~~15~~), viscoelastic coefficient (Eq. 17~~16~~) and plastic multiplier (Eq. 18~~17~~) can be substituted into pressure equation (Eq. 14~~13~~) and deviatoric stress equation (Eq. 15~~14~~). Together with mechanical equilibrium equation (Eq. 13~~12~~), they form a system of three equations with three unknowns, namely $\bar{v}_r$, ~~$\overline{\tau_{rr}}$ and $\bar{P}$.~~$\overline{\tau_{rr}}$ and $\bar{P}$. The numerical model is based on a finite-difference scheme over 1D staggered grid (numerical stencil see e.g. Gerya (2010) chapter 7). The initial pressure $\bar{P}$ is set at the beginning of the numerical model. If upon entrapment, the inclusion and host possess the same hydrostatic pressure, the deviatoric stress $\overline{\tau_{rr}}$ is zero in the inclusion and host. If pressure heterogeneity exist upon entrapment, the deviatoric stress of the host ($\overline{\tau_{rr}}$) needs to be pre-calculated with elastic model $\overline{\tau_{rr}} = -(P_{\text{inc}} - P_{\text{host}})/\bar{r}^3$ to ensure that mechanical equilibrium is satisfied at the beginning of the model ($P_{\text{inc}}$ is the initial inclusion pressure and $P_{\text{host}}$ is the initial host pressure).

For pre-defined *P-T* path, the inclusion-host system is loaded by the increment of confining pressure and temperature. Both temperature and far-field pressure are obtained directly from the *P-T-t* path as prescribed. Temperature is treated as

homogeneous in the model and the new pressure is set as the outer boundary value. Because viscosity, viscoelastic coefficient and plastic multiplier are functions of deviatoric stress~~,~~ (viscosity is also a function of temperature as prescribed by the *P-T* path), the system of the mechanical equations is nonlinear. We solve for the three variables ($\bar{v}_r$, $\overline{\tau_{rr}}$ and $\bar{P}$) using an iterative (Picard) method. Within the iteration loop, an elastic test stress is first evaluated by letting $\bar{\lambda} = 0$ so that the prediction for the yield function $\bar{F}$ is ~~computed~~obtained. If $\bar{F} < 0$, no plastic yield occurs and $\bar{\lambda}$ ~~is~~ remains zero. Otherwise the prediction of the yield function is positive and $\bar{\lambda}$ is computed based on Eq.18~~17 to drive $\bar{F}$ back to zero.~~. The calculated $\bar{\lambda}$ is then substituted back into Eq. 15 to adjust the amount of plastic strain rate. This will drive $\bar{F}$ to zero (on the plastic yield surface). After the Picard iteration loop, the residuals of the three equations 13, 14 and 15 are minimized below ca. $10^{-12}$.

The elastic moduli are updated based on pressure and temperature conditions from tabulated look-up tables within the iteration. The look-up tables are pre-computed based on EoS. We used the EoS for quartz crystal from Angel et al. (2017a), and the EoS for pyrope, grossular and almandine crystals from Milani et al. (2015). The detailed expressions of EoS can be found in the EoSFit7c software documentation (Angel et al., 2014). The EoS for spessartine is from Gréaux and Yamada, (2014). The compressibility and thermal expansion coefficient for garnet are averaged based on the molar percentage of garnet endmembers. The shear moduli of garnet endmembers are from Bass (1995). ~~The host radius is set to be 10~~The numerical model has been benchmarked using the analytical solution with elastic, non-Newtonian viscous rheology in Zhong et al., (2018).~~ times the inclusion radius to make boundary effects negligible. Temperature is treated as homogeneous in space.~~ ~~After the iteration loop, the residuals of the three equations 12, 13 and 14 are minimized below ca. $10^{-12}$. The numerical model has been benchmarked using the analytical solution with elastic, non-Newtonian viscous rheology in Zhong et al., 2018.~~ The numerical benchmark for elasto-plastic rheology is performed by using the analytical solution of Zhang, (1998) (see supplementary materials).

## ~~2.4 Analytical solution of inclusion~~ 3. Inclusion pressure ~~close~~modification due to ~~thin section surface~~visco-plastic deformation of host

~~Pressure relaxation takes place when the inclusion is brought into proximity to a stress-free thin section surface. Mindlin and Cheng (1950) provided a closed-form analytical solution of stress field inside and outside a spherical inclusion with thermal strain in a semi-infinite host. The analytical solution has been generalized to ellipsoidal inclusion (Seo and Mura, 1979).~~

Substantial mathematical investigations have also been done in deriving the analytical solution of the elastic field for inclusion in half space (e.g. Tsuchida and Nakahara, 1970; Aderogba, 1976; Jasiuk et al., 1991). In this work, a simplified analytical formulation of pressure field within a spherical inclusion $P_{inc}$ close to thin section surface is given. It is emphasized that in this situation the inclusion and host possess the same elastic moduli and the residual pressure is caused only by thermal expansion/contraction. The goal here is to analytical demonstrate the effect of inclusion's proximity to the thin section surface. Cartesian coordinate system is employed as shown in Fig. 2. The full stress tensor $\sigma_{ij}$ of inclusion loaded with eigenstrains is represented as follows (Seo and Mura, 1979).

$$\sigma_{ij} = \frac{\varepsilon^*(1+\nu)G}{2\pi(1-\nu)}\left[-4\pi\delta_{ij} - \frac{\partial^2\psi}{\partial x_i x_j} + 4\nu\delta_{ij}\frac{\partial^2\phi}{\partial x_3 x_3} + (3-4\nu)\left(\delta_{3j}+\delta_{3j}-1\right)\frac{\partial^2\phi}{\partial x_i x_j} - \left(\delta_{3j}+\delta_{3j}\right)\frac{\partial^2\phi}{\partial x_i x_j} - 2x_3\frac{\partial^3\phi}{\partial x_3 x_i x_j}\right]. \quad (20)$$

While for the host, stresses are given below

$$\sigma_{ij} = \frac{\varepsilon^*(1+\nu)G}{2\pi(1-\nu)}\left[-\frac{\partial^2\psi}{\partial x_i x_j} + 4\nu\delta_{ij}\frac{\partial^2\phi}{\partial x_3 x_3} + (3-4\nu)\left(\delta_{3j}+\delta_{3j}-1\right)\frac{\partial^2\phi}{\partial x_i x_j} - \left(\delta_{3j}+\delta_{3j}\right)\frac{\partial^2\phi}{\partial x_i x_j} - 2x_3\frac{\partial^3\phi}{\partial x_3 x_i x_j}\right], \quad (21)$$

where the indices of $x_i$ ($i = 1,2,3$) are in Cartesian coordinate frame following the order of $x$, $y$ and $z$ (see Fig. 2), and $\varepsilon^*$ is the isotropic eigenstrain that is expressed as the difference of volumetric strain between inclusion and host assuming that they are not bounded by each other. As the inclusion and host possess the same elastic moduli, the difference of volumetric strain is only caused by the thermal expansion coefficient difference.

$$\varepsilon^* = -\frac{\Delta T(\alpha_i - \alpha_h)}{3}. \quad (22)$$

The elliptic integrals $\psi$ and $\phi$ are expressed below:

~~$$\psi = \pi R^3 \int_{\lambda}^{\infty} \frac{1-\frac{R_1^2}{R^2+s}}{(R^2+s)^{\frac{3}{2}}} ds,$$~~ ~~(23)~~

~~where $\lambda = R_1^2 - R^2$ for host, $\lambda = 0$ for inclusion, and $R_1 = \sqrt{x_1^2 + x_2^2 + (x_3 - L)^2}$.~~

~~$$\phi = \pi R^3 \int_{\lambda}^{\infty} \frac{1-\frac{R_2^2}{R^2+s}}{(R^2+s)^{\frac{3}{2}}} ds,$$~~ ~~(24)~~

~~where $\lambda = R_2^2 - R^2$ for both host and inclusion, and $R_2 = \sqrt{x_1^2 + x_2^2 + (x_3 + L)^2}$.~~ ~~Here, we focus on inclusion and derive a simplified form for the pressure of inclusion. For the inclusion, the elliptic integrals are derived:~~

~~$$\psi = 2\pi\left(R^2 - \frac{1}{3}R_1^2\right),$$~~ ~~(25)~~

~~$$\phi = \frac{4}{3}\pi R^3 R_2^{-1}.$$~~ ~~(26)~~

~~The normal stresses in the inclusion are:~~

~~$$\sigma_{11} = \frac{\epsilon^*(1+\nu)G}{2\pi(1-\nu)}\left[-4\pi - \frac{\partial^2\psi}{\partial x_1 x_1} + 4\nu\frac{\partial^2\phi}{\partial x_3 x_3} - (3-4\nu)\frac{\partial^2\phi}{\partial x_1 x_1} - 2x_3\frac{\partial^3\phi}{\partial x_3 x_1 x_1}\right],$$~~ ~~(27)~~

~~$$\sigma_{22} = \frac{\epsilon^*(1+\nu)G}{2\pi(1-\nu)}\left[-4\pi - \frac{\partial^2\psi}{\partial x_2 x_2} + 4\nu\frac{\partial^2\phi}{\partial x_3 x_3} - (3-4\nu)\frac{\partial^2\phi}{\partial x_2 x_2} - 2x_3\frac{\partial^3\phi}{\partial x_3 x_2 x_2}\right],$$~~ ~~(28)~~

~~$$\sigma_{33} = \frac{\epsilon^*(1+\nu)G}{2\pi(1-\nu)}\left[-4\pi - \frac{\partial^2\psi}{\partial x_3 x_3} + 4\nu\frac{\partial^2\phi}{\partial x_3 x_3} + (3-4\nu)\frac{\partial^2\phi}{\partial x_3 x_3} - 2x_3\frac{\partial^3\phi}{\partial x_3^3} - 2\frac{\partial^2\phi}{\partial x_3^2}\right].$$~~ ~~(29)~~

~~**By substituting $\psi$ and $\phi$ into the equations above, the normal stresses can be obtained. In deriving the pressure, i.e. negative mean stress, many terms in Eq. 27-29 can be cancelled out.**~~ **3.1 Residual pressure affected by viscous/plastic flow**

The solutions of the system of ~~A simplified form is obtained as follow:~~

$$P_{inc} = \frac{4\epsilon^*(1+\nu)G}{3(1-\nu)}\left[1 - \frac{2}{3}\frac{R^3}{R_2^3}(1+\nu)\left(\frac{3(z+L)^2}{R_2^2} - 1\right)\right]. \quad (30)$$

Substituting the eigenstrain $\epsilon^*$ and the expression of $P_{exp}$ in Eq. 10 into pressure, we obtain:

$$P_{inc} = P_{exp}[1 - \frac{2}{3}\frac{R^3}{R_2^3}(1+\nu)(\frac{3(z+L)^2}{R_2^2} - 1)]. \quad (31)$$

The equation can be nondimensionalized by(Eq. 13, 14, 15) are obtained using the elasticity of quartz-in-garnet system. The host radius is set to be 50 times the inclusion radius to make boundary effects negligible. Temperature is treated as homogeneous in space. $R$ as length scale shown below:

$$\frac{P_{inc}}{P_{exp}} = 1 - \frac{2}{3}\frac{1+\nu}{\bar{R}_2^3}(\frac{3(\bar{z}+\bar{L})^2}{\bar{R}_2^2} - 1). \quad (32)$$

The analytical solution for pressure in the mineral inclusion subject to an initial residual pressure $P_{exp}$ is obtained. When the inclusion is far from thin-section surface ($\bar{L} \to +\infty$, and $\bar{R}_2 \to +\infty$), the actual residual pressure approaches the expected residual pressure based on classical elastic model ($P_{inc} \to P_{exp}$). The pressure field of an inclusion in half space based on Eq. 32 is shown in Fig. 2 using the Poisson ratio $\nu$ of pyrope crystal.

## 3. Results

### 3.1 Systematic investigation on Deborah number and Cohesion number

At the beginning of the model, a pressure perturbation within the inclusion is prescribed, and the far-field host maintains zero confining pressure. The pre-factor of viscosity is fixed as temperature does not vary in this case. The amount of inclusion pressure relaxation is systematically investigated for the two inelastic deformation mechanisms (i.e. viscous creep and plastic yield) as a function of $De$ and $C^*$. At the beginning of the model, a residual pressure with the inclusion is prescribed, and the far field host maintains zero confining pressure. The pre factor of viscosity is fixed as temperature does not vary. TheThe results are shown in Fig. 2 with the purpose of this diagram in Fig. 3 is to systematically demonstratedemonstrating how much

the initially prescribed residual pressure can be ~~relaxed~~reduced due to viscous creep and plastic yield ~~as controlled by $De$ and $C^*$.~~. This diagram may assist petrological investigations because $De$ and $C^*$ can be evaluated based on experimental rock deformation data for different minerals~~, and they can be used with the diagram to check if viscous relaxation and plastic yield are expected or not.~~

~~The computed residual inclusion pressure is shown in Fig. 3.~~. The Deborah number can be evaluated using experimental flow law of single crystal, e.g. garnet (Karato et al., 1995; Wang and Ji, 1999) as given in the next section. The plastic yield strength is evaluated using microhardness test data (see Discussion below for details). The thickness of plastic yield region is plotted as contours. The thick grey contour represents the onset of plastic yield starting from the inclusion-host interface and propagating towards the host side (Fig. ~~3~~2). Based on the amount of inclusion pressure relaxation, three regimes are distinguished.

***Elastic regime*** takes place when $De$ and $C^*$ are higher than one. Under these circumstances, no viscous relaxation and plastic yield occurs. The residual inclusion pressure is close to the expected residual pressure ($\sout{P_{inc}}P_{\mathrm{inc}} \approx \sout{P_{exp}}P_{\mathrm{exp}}$). This regime is the most suitable for the application of Raman-thermobarometry.

***Viscous regime*** dominates when $De$ is lower than one, and $C^*$ is above the plastic onset shown by the thick grey contour. In this case, the main mechanism responsible for the inclusion pressure relaxation is the viscous creep. The effect of stress exponent on the amount of viscous relaxation is also significant. In general, a higher stress exponent delays pressure relaxation (c.f. Dabrowski et al., 2015). As the viscosity of natural minerals is low at high temperature conditions, the viscous regime may be reached at high temperature ~~that~~which leads to the relaxation of residual pressure.

***Plastic regime*** prevails when $C^*$ is lower than one~~,~~ and $De$ is ~~located~~ above ~~the plastic onset~~one. Under this circumstance, the residual pressure is not significantly relaxed by viscous creep, but by plastic yield. In general, the radius of plastic yield region is positively related to amount of residual pressure ~~relaxation~~release.

### 3.2 Pressure relaxation due to free surface

As a case study, the stress fields of quartz in almandine and almandine in quartz systems are numerically modelled using a finite-difference (FD) thermo-elastic model (governing equations and model benchmark are provided in supplementary material). These examples are chosen to investigate two end-members: elastically stiffer host (quartz in almandine in Fig. 4a) and softer host (almandine in quartz in Fig. 4b). Pressures at three points within the inclusion (top, centre and bottom) are contoured as a function of $\bar{L}$ (see Fig. 4). The pressures evaluated at these three localities based on the analytical solution in Eq. 32 are also shown by the dashed curves for comparison with numerical solutions. With decreasing distance to thin-section surface, the heterogeneity of pressure field increases. The pressure at the top point relaxes the most. Meanwhile, non-negligible pressure relaxation also takes place at the centre and bottom points. It is shown that pressure relaxation is less significant in elastically stiffer host (garnet) than in elastically softer host (quartz).

It is shown that the difference between analytical and numerical solution due to the difference of elastic moduli becomes significant when the inclusion depth is shallow. The analytical solution and numerical solution are similar when evaluated at the bottom point at any depth. For quartz in garnet system, the analytical solution overestimates the amount of pressure relaxation (Fig. 4a). Assuming 3% pressure relaxation as acceptable for the application of Raman barometry, the analytical solution yields safe distance ca. $\bar{L}$=2.0 for the bottom and centre point, while the numerical solution yields ca. $\bar{L}$=1.5. For the top point, the safe distance ca. $\bar{L}$=2.5 based on the analytical solution is again higher than the prediction of ca. $\bar{L}$=2.0 based on numerical solution. The difference of safe distance between analytical and numerical solution is due to the presence of elastically stiffer garnet host.

Differential stress is also shown in Fig. 4b. High differential stress at the host appears when the inclusion is close to thin-section surface. Differential stress may also exist inside the inclusion but it is in general smaller than that of the host. For quartz in garnet system, the differential stress forms a "ring" shaped pattern with a peak at the surface. The differential stress may reach up to three times the expected residual pressure. This may potentially trigger plastic failure at thin-section surface. However, for the garnet-in-quartz system, such pattern is not observed even if the inclusion depth is shallow.

~~**3.3 Viscous relaxation of quartz-in-garnet system**~~

It is noted here that although viscous relaxation and plastic yield of the host mineral have the same effect in reducing the residual inclusion pressure after exhumation, there is a fundamental difference between them. Viscous relaxation is time-dependent (*De* includes time), which means that the residual pressure will vanish given infinite amount of time. Plastic yield refers to a time-independent process and it will only limit the amount of deviatoric stress supported by the host mineral. If the yield criterion is reached, plastic strain (rate) in the host immediately occurs which leads to the inclusion pressure release. Both viscous relaxation and plastic yield are non-reversible, i.e. if the inclusion-host system is placed back to the original entrapment condition, the stress state would be different.

**3.2 Viscous relaxation of garnet host**

Assuming that the thin-section surface is sufficiently far away from a quartz inclusion and no ~~microcracks appear~~plastic yield occurs around the quartz inclusion, ~~only~~ viscous creep may only contribute to the ~~relaxation~~modification of residual pressure. Here, we show the effect of viscous relaxation, particularly influenced by the temperature, on the preserved residual pressure. Using *De* as a criterion to estimate the amount of viscous relaxation ~~(Fig. 3),~~ we show the relationship between temperature, inclusion pressure, and relaxation time given *De*=1 (see Eq. 19~~18~~) in Fig. ~~5~~3. The flow law of garnet from Wang and Ji (1999) is applied. The ~~flow law parameters are given~~pre-factor $A$ of the effective viscosity (Eq. 4) is as follows:

$$A = \frac{G^n}{2B}\exp\left(\frac{g \cdot T_m}{T}\right), \quad (21)$$

where $B = \exp(40.1)$ in ~~the figure caption.~~$s^{-1}$, $g = 32$. The stress exponent $n = 3$. Geometric correction based on experimental setup (simple/pure shear) was not applied. The melting point $T_m$ of pyrope-rich garnet, grossular and spessartine are from the Table 1 in Karato et al. (1995). For almost pure almandine, the garnet melting point is found to be 1588 K from Mohawk Garnet Inc, which is slightly higher than 1570 K for almandine rich ($Alm_{0.68}Prp_{0.20}Grs_{0.12}$) garnet in Karato et al. (1995).

As an example~~,~~ (Fig. 3), for a quartz inclusion possessing 0.5 GPa residual pressure maintained at 650 °C, significant viscous relaxation ~~will occur~~is expected during 1 Ma for almandine rich garnet host based on the applied flow law. This temperature

becomes higher (700 ºC) for pyrope rich garnet. If the residual pressure is used to recover the entrapment pressure given that the temperature experienced by the garnet-host system was higher than 650~700 ºC, an underestimate of the entrapment pressure may potentially occur.

In Fig. ~~6~~4, synthetic retrograde *P-T* paths from eclogite and amphibolite-facies metamorphic conditions are prescribed with different peak temperature. The entrapment *P-T* conditions for the three synthetic *P-T* paths are along an elastic ~~isomekes~~isomeke, which ~~are~~is the ~~isopleths of residual~~isopleth where no relative elastic interaction exists between inclusion ~~pressure as a function of entrapment *P-T* conditions. Therefore~~and host. Thus, the residual inclusion pressure ~~should~~would be the same if ~~viscous relaxation is not considered.~~the inclusions were entrapped along the same isomeke and they were purely elastic. By involving the viscous rheology of the garnet host, different residual inclusion pressures are predicted. For the *P-T* path starting at 800 ºC, 2 GPa, the quartz inclusion pressure is predicted to be less than 0.2 GPa. ~~The~~ This reduced value of the residual ~~inclusion~~ pressure ~~subject to viscous relaxation is~~is then used to determine the apparent entrapment pressure (Fig. ~~6b~~4b). In Fig. ~~6b~~4b, it is shown that for the entrapment pressure within eclogite-facies conditions at 700 ºC, and by using ~~only the~~ a purely-elastic model, a value of entrapment pressure is inferred that is approximately 10% less than the actual value. The amount of ~~underestimate~~underestimation of entrapment pressure increases to 30% when the entrapment temperature reaches 800 ºC. ~~The~~These values are conservative estimates since the total exhumation time is set as 1 Ma. Longer residence at high-temperature conditions would result to larger modifications of the residual pressure.

For amphibolite-facies entrapment conditions, the residual pressure that is preserved in the quartz inclusion is significantly lower compared to the case where the entrapment occurred at eclogites-facies conditions. ~~In this case, the amount of underestimate is less as well due to the fact that the viscosity of garnet host is stress dependent (see Eq. 5). As shown in Fig. 6D~~As shown in Fig. 4D, ca. 5% and 20 % underestimate of true entrapment pressure is predicted depending whether the entrapment occurred at 700 ºC or 800 ºC, respectively. Similarly, the amount of underestimation will be larger if the duration of exhumation is longer than 1Ma.

### 3.43 Pressure relaxation along prograde P-T path and apparent overstepping

The pressure relaxation problem ~~is~~becomes more complicated when the quartz inclusion is entrapped not at the peak *P-T* conditions, but along the prograde *P-T* path. In this case, viscous relaxation occurs also along the prograde *P-T* path and the pressure difference between host and inclusion will relax with time and increasing temperature. This effect starts before the rock reaches the peak *P-T* conditions. Two synthetic *P-T* paths are illustrated in Fig. ~~7~~5. In Fig. ~~7a~~5a, the quartz is entrapped in the almandine-garnet host at 400 ºC, 1 GPa and further experiences eclogites-facies *P-T* conditions. During the prograde path, the quartz inclusion will develop underpressure~~,~~ (e.g. Angel et al., 2015, Fig. 5), which will also be subject to viscous relaxation over geological time. The quartz pressure starts to converge towards the garnet host pressure at *T*>600 ºC. Nearly complete viscous resetting is observed when the system is brought up to 800 ºC. The prograde time is set as 1 Ma or 10 Ma to compare the amount of viscous relaxation as a function of time in Fig. ~~7~~5.

~~The~~An alternative scenario is considered where the rock may also stay at the peak *P-T* conditions before decompression occurs. A synthetic clockwise *P-T* path reaching eclogite facies metamorphic condition is constructed as shown in Fig. ~~8~~6. The quartz inclusion is entrapped into the garnet host at 400 ºC, 0.6 GPa, which is considered to be along the entrance of garnet stability field. Subsequently the system is brought to 700~750 ºC, 1.8~1.9 GPa conditions and stays there for 5 Ma. Afterwards, the retrograde *P-T* path takes 10 Ma. Two different *P-T* paths of quartz inclusions are constructed based on the implemented elastic and visco-elastic rheologies. Interestingly, the residual pressure of the inclusion that was subject to viscous relaxation is significantly higher (by 0.2 GPa,) than the prediction of pure elastic model as shown by the black dashed curve (0.14 GPa). The apparent entrapment pressure is calculated using the predicted residual pressure for the inclusion whose host experienced viscous relaxation. A large discrepancy exists between the apparent entrapment pressure (ca. 1 GPa at the entrapment *T* 400 ºC) and the true entrapment pressure (0.6 GPa). The overall overestimate of true entrapment pressure (0.6 GPa) is about 0.3~0.4 GPa, which may potentially be interpreted as overstepping of the garnet growth/nucleation.

## 4. ~~Discussion~~Inclusion pressure modification due to proximity to thin-section surface

Despite the importance of viscous/plastic relaxation in the post-entrapment modification of pressure, residual pressure measurements may be different when the inclusions are closer to the thin-section surface (Enami et al., 2007). When a

pressurized mineral inclusion in infinite host under mechanical equilibrium is moved towards the thin-section surface, its pressure is released and the pressure distribution within the inclusion becomes heterogeneous. Mindlin and Cheng (1950) provided a closed-form analytical solution of stress field inside and outside a spherical inclusion with thermal strain in a semi-infinite host. The analytical solution has been generalized to ellipsoidal inclusion (Seo and Mura, 1979). Substantial mathematical investigations have also been done in deriving the analytical solution of the elastic field for inclusion in half-space (e.g. Tsuchida and Nakahara, 1970; Aderogba, 1976; Jasiuk et al., 1991). Although the analytical formulations for individual stress components of inclusion are non-trivial, here, we show that the formula for pressure distribution of a pressurized inclusion can be significantly simplified (detailed derivations are provided in the Appendix):

$$\frac{P_{\text{inc}}}{P_{\text{ini}}} = 1 - \frac{2}{3}\frac{1+\nu}{\bar{R}_2^3}\left(\frac{3(\bar{z}+\bar{L})^2}{\bar{R}_2^2} - 1\right). \quad (22)$$

where $P_{\text{ini}}$ is the initial inclusion pressure in infinite host under mechanical equilibrium, $\bar{L}$ is the scaled inclusion depth ($\bar{L} = L/R$) and $\bar{R}_2 = \sqrt{x_1^2 + x_2^2 + (x_3 + L)^2}/R$ is a function of position in Cartesian coordinate system (Fig. 7), $\nu$ is the Poisson ratio of the inclusion and host. It is emphasized that in this situation the inclusion and host possess the same elastic moduli.

The released inclusion pressure due to proximity to the thin-section surface is plotted in Fig. 7b and 7c using Eq. 22. Pressure release is concentrated at the top of the inclusion while the bottom of the inclusion is subject to minimal pressure releases (<10%). Interestingly, the top of the inclusion is subject to negative pressure (expansion) when the inclusion is very close to the thin-section surface (e.g. see the case of $\bar{L} = 1.1$). Based on the analytical solution, the safe inclusion depth to avoid residual pressure release is ca. $\bar{L} = 2.5$ (the amount of pressure release is less than 3% within the entire inclusion). Here, the simple analytical solution in Eq. 22 can precisely model the inclusion's residual pressure due to stress release at thin-section surface, where the inclusion possesses the same elastic moduli as the host. In natural mineral inclusion-host system, the inclusion and host possess different elastic properties. As a case study, the stress fields of quartz-in-almandine and almandine-in-quartz systems are numerically modelled using a finite difference (FD) thermo-elastic model (model benchmark are provided in supplementary material). These examples are chosen to investigate two end-members: elastically stiffer host (quartz-in-almandine in Fig. 8a) and softer host (almandine-in-quartz in Fig. 8b). Pressures at three points within the inclusion (top, centre and bottom) are contoured as a function of $\bar{L}$. The pressures evaluated at these three localities based on the analytical solution

in Eq. 22 are also shown by the dashed curves for comparison with numerical solutions. With decreasing distance to thin-section surface, the heterogeneity of pressure field increases. It is shown that the pressure release is less significant in elastically stiffer host (garnet) than in elastically softer host (quartz).

It is shown that the difference between analytical and numerical solution due to the difference of elastic moduli becomes significant when the inclusion depth is shallow. The analytical and solutions are similar when evaluated at the bottom point at any depth (Fig. 8). For quartz-in-garnet system, the analytical solution overestimates the amount of pressure release (Fig. 8a). Assuming 3% pressure release as acceptable for the application of Raman barometry, the analytical solution yields safe distance ca. $\bar{L}$=2.0 for the bottom and centre point, while the numerical solution yields ca. $\bar{L}$=1.5. For the top point, the safe distance ca. $\bar{L}$=2.5 based on the analytical solution is again higher than the prediction of ca. $\bar{L}$=2.0 based on numerical solution. The difference of safe distance between analytical and numerical solution is due to the presence of elastically stiffer garnet host.

Differential stress ($|\sigma_1 - \sigma_3|$) is also shown in Fig. 8b. High differential stress at the host appears when the inclusion is close to thin-section surface. Differential stress may also exist inside the inclusion but it is in general smaller than that of the host. For quartz-in-garnet system, the differential stress forms a "ring" shaped pattern with a peak at the surface. The differential stress may reach up to three times the expected residual pressure. This may potentially trigger plastic failure at thin-section surface. However, for the garnet-in-quartz system, such pattern is not observed even if the inclusion depth is shallow.

## 45. Discussion

### 5.1 What may cause the residual pressure ~~relaxation~~modification?

The ~~three~~ mechanisms investigated here, i.e. ~~viscous creep,~~ visco-plastic ~~yield~~flow of the host and proximity of inclusion to thin-section surface can all be responsible for the ~~relaxation~~modification of the residual inclusion pressure. The amount of inclusion-pressure ~~relaxation~~change due to these three mechanisms is controlled by Deborah number ($De$), ~~Cohesion number~~dimensionless yield strength ($C^*$) and dimensionless depth ($\bar{L}$), respectively. ~~These three numbers are recommended to be examined beforehand.~~

In the examples of quartz-in-garnet systems, the residual pressure is considered to be sealed in ~~creak-free garnet host. However, cracks have been observed around some quartz inclusions but those inclusions are often avoided (e.g. Ashley et al., 2014; Kouketsu et al., 2016).~~perfectly elastic garnet host. Based on our study, the presence (radius) of plastic yield region and preserved residual inclusion pressure are dominated by ~~Cohesion number~~dimensionless yield strength ($C^* = C_h/P_{exp}P_{\mathrm{exp}}$) as shown in Fig. ~~3. Cohesion~~2. Strength $C_h$ can be converted from hardness test data using the formula below (e.g. Evans and Goetze, 1979):

$$C_h = H/C_g \qquad (23\sout{233})$$

where $H$ is the measured microhardness and $C_g$ is a constant accounting for the indenter's geometry in the experiment. Taking $C_g = 3$ (Evans and Goetze, 1979), the ~~cohesion~~yield strength of garnet host is between 4.4 and 5 GPa at room conditions (Whitney et al., 2007), which leads to ~~a Cohesion number~~ $C^* = 4.4{\sim}5$ given residual inclusion pressure $P_{exp}P_{\mathrm{exp}} = 1$ GPa. This suggests that plastic yield does not occur in an idealized scenario of isotropic, spherical quartz inclusion entrapped in infinite garnet host. However, such an ideal scenario is highly improbable in natural samples. ~~The observed cracks in garnet host~~Localized plastic yield may ~~be formed~~still occur due to ~~potential~~following reasons ~~including~~: 1) elevated differential stress when the inclusion is close to thin-section surface ("ring" shaped pattern in Fig. ~~4a~~8); 2) stress concentration at the corners of quartz inclusion (Whitney et al., 2000); 3) anisotropic elastic deformation of the quartz inclusion (e.g. Murri et al., 2018); 4) pre-fractures/weakness in garnet host before the entrapment of quartz inclusions~~.~~ that leads to the localization of dislocations. Although our model does not predict exact conditions for plastic yield due to the above possibilities, it gives a lower bound for the ~~cohesion~~strength and provides information on what type of host mineral phase cannot be used for Raman-barometry. ~~Cohesion data~~Plastic yield strength of some common rock-forming minerals measured in hardness tests are compiled and provided in table 1. As an example, given $P_{exp}P_{\mathrm{exp}} = 1$ GPa, the ~~Cohesion number~~dimensionless yield strength of calcite host is ca. 0.6, and dolomite is ca. 1.5 (Wong and Bradt, 1992). ~~This implies that calcite will partially relax the residual pressure $P_{exp}$ and dolomite has the potential to preserve $P_{exp}$. Care must be taken to check the potential presence of microcracks around inclusions when using host minerals with low Cohesion number for Raman-barometry, e.g. zircon, dolomite. Minerals such as~~

~~calcite should be avoided to be used as the host material for the application of Raman barometry.~~ This implies that plastic flow will most likely affect the residual pressure $P_{exp}$ in the calcite host but not in dolomite host.

After thin-section preparation, the inclusion pressure may be (partially) ~~relaxed~~released. The dimensionless depth can be evaluated by performing depth-step scan analysis with Raman spectroscopy in order to observe if the pressure gradually decreases towards thin-section surface ~~(Enami et al., 2007; Campomenosi et al., 2018). For quartz-in-garnet system, to avoid significant pressure relaxation~~(Enami et al., 2007). For quartz-in-garnet system, to avoid significant pressure release (>3%) in the bottom half of inclusion, the dimensionless depth needs to be above at least 1.5 (Fig. ~~4~~8). To avoid significant pressure ~~relaxation~~release in the entire quartz inclusion, the dimensionless depth needs to be above ~2. Therefore, we recommend a safe dimensionless depth of ~~~2~~2~2.5 (from surface to the centre of inclusion) for quartz-in-garnet Raman-barometry (see also Mazzucchelli et al., 2018). For a 30 μm thick thin-section, the maximal radius of an inclusion is ca. 6 μm (12 μm in diameter) located at the mid-point of the thin-section. In practice, it is difficult to precisely measure the depth of an inclusion and it is uncommon that an inclusion is located right in the middle of a thin-section. Therefore, it is ideal to choose smaller inclusions or prepare thicker thin-section for measurement (Campomenosi et al., 2018; Mazzucchelli et al., 2018).

For commonly used quartz-in-garnet Raman-barometry, our results show that below 550~600 °C, the effect of viscous relaxation can be negligible. Above ca. 650~750 °C, the effect of viscous relaxation needs to be taken into account depending on particular *P*-*T* path, garnet composition and time scale (Fig. ~~5~~3, Fig. ~~6~~4). This is similar to the empirical estimate ca. 750 °C in Walters and Kohn (2014). It is also shown that the preserved residual pressure may even increase due to viscous relaxation if viscous resetting occurs at peak *P* condition (Fig. ~~8~~6). This is simply because viscous creep does not only relax the overpressure in quartz inclusion, but also the underpressure that develops along prograde *P*-*T* path. Meanwhile, the amount of viscous relaxation is time-dependent ($De$ is a function of the operating time of viscous relaxation). Thus, the above temperature criterion for Raman-barometry applies only for exhumation lasting at million years' time scale. A higher temperature criterion for Raman-barometry (e.g. ~1000 °C for garnet host at high pressure close to coesite-quartz transition) is applicable for more rapid exhumation, e.g. xenolith ascent carried by magma (Zhong et al., 2018b) or garnet synthesis experiments that lasts hours/days (Thomas and Spear, 2018; Bonazzi et al., 2019).

### 45.2 Implications to garnet overstepping

Quartz-in-garnet Raman-barometry has been used to determine the entrapment pressure, i.e. garnet nucleation/growth conditions and compared to the *P-T* conditions determined based on phase equilibria/classical chemical thermobarometry (Castro and Spear, 2017; Spear et al., 2014). As has been shown in Fig. 86, viscous resetting occurs when the inclusion-host system is brought to high temperature (>600~700 ºC). Even if the quartz inclusion is entrapped at lower *P-T* conditions, e.g. the garnet entrance conditions, the preserved residual inclusion pressure may still be significantly higher than predicted from the actual entrapment *P-T* conditions using pure elastic model. In this case, erroneous results may emerge if one uses the relaxed residual quartz inclusion pressure to determine the entrapment pressure. In case of significant viscous resetting at peak *T* conditions followed by decompression, as in the case of some HP rocks, apparent garnet growth overstepping will be inferred (see Fig. 8b). Care6b). In that case, care must thus be taken to interpret the discrepancy between the results of quartz-in-garnet Raman barometry and phase equilibria. As shown in the example with synthetic clockwise *P-T* path (Fig. 86), ca. 3~4 kbar apparent overstepping is yieldedpredicted by considering viscous resetting at peak *T* condition. The amount of apparent overstepping will be even larger if the exhumation process happens faster (current model assumes 10 Ma decompression time).

## 56. Conclusions

We first presented a 1D visco-elasto-plastic model to study the inclusion-host system undergoing a prograde/retrograde *P-T* path. NondimensionalizationThe nondimensionalization of the governing equations yields two controlling parameters, Deborah number (*De*) and cohesion numberdimensionless yield strength ($C^*$) that control the amount of pressure drop due to viscous relaxation and plastic relaxation of the residual pressure of inclusion.yield. Both *De* and $C^*$ must be higher than one to avoid relaxation due to viscous creep and plastic yield. Aunderestimating the residual pressure. Subsequently, a simplified analytical solution for inclusion pressure (Eq. 3222) close to stress-free thin-section surface is derived.presented based on the existing analytical solution from Seo and Mura (1979). It is suggested that the distance between thin-section surface and inclusion must be higher than 2~3 times the inclusion radius to avoid stress relaxationrelease.

The relevance of our presented visco-elasto-plastic model to quartz-in-garnet elastic barometry has been systematically studied. Although plastic yield is not expected for garnet host due to its high yield strength, the residual inclusion pressure preserved

in quartz inclusion can be partially modified at high temperature due to time-dependent viscous creep. It is shown that above 650~700ºC over Ma time scale, viscous creep of garnet host may partially reset the quartz pressure. This may have important implications for the determination of entrapment pressure of quartz inclusion. Additionally, this may also cause apparent overstepping of garnet growth, thus care must be taken when applying quartz-in-garnet barometry at rocks which experienced high temperatures (>600~700 ºC).

**Code availability**

The MATLAB code to reproduce the results of quartz-in-garnet system is ~~uploaded with the paper~~available upon request.

**Author contribution**

X.Z. designed the numerical/analytical model and wrote the MATLAB code. All the co-authors contributed in discussion and wrote the manuscript together.

**Competing interests**

The authors declare no conflict of interest.

**Acknowledgements**

This work is supported by MADE-IN-EARTH ERC starting grant (n.335577) to LT and Swiss National Science Foundation (P2EZP2_172220) to XZ. We thank V. Yarushina and an anonymous reviewer for helpful comments that greatly improved the quality of this work.

**Appendix**

Here, we introduce a simplified formula for pressure distribution of an initially pressurized inclusion in infinite host moved toward a stress-free surface based on the existing analytical solution of Seo and Mura (1979). A Cartesian coordinate system

is employed as shown in Fig. 7. The full stress tensor $\sigma_{ij}$ of inclusion loaded with eigenstrains is represented as follows (Seo and Mura, 1979).

$$\sigma_{ij} = \frac{\varepsilon^*(1+\nu)G}{2\pi(1-\nu)}\left[-4\pi\delta_{ij} - \frac{\partial^2\psi}{\partial x_i x_j} + 4\nu\delta_{ij}\frac{\partial^2\phi}{\partial x_3 x_3} + (3-4\nu)\left(\delta_{3j}+\delta_{3j}-1\right)\frac{\partial^2\phi}{\partial x_i x_j} - \left(\delta_{3j}+\delta_{3j}\right)\frac{\partial^2\phi}{\partial x_i x_j} - 2x_3\frac{\partial^3\phi}{\partial x_3 x_i x_j}\right]. \quad \text{(A1)}$$

While for the host, stresses are given below

$$\sigma_{ij} = \frac{\varepsilon^*(1+\nu)G}{2\pi(1-\nu)}\left[-\frac{\partial^2\psi}{\partial x_i x_j} + 4\nu\delta_{ij}\frac{\partial^2\phi}{\partial x_3 x_3} + (3-4\nu)\left(\delta_{3j}+\delta_{3j}-1\right)\frac{\partial^2\phi}{\partial x_i x_j} - \left(\delta_{3j}+\delta_{3j}\right)\frac{\partial^2\phi}{\partial x_i x_j} - 2x_3\frac{\partial^3\phi}{\partial x_3 x_i x_j}\right]. \quad \text{(A2)}$$

where the indices of $x_i$ ($i = 1,2,3$) are in Cartesian coordinate frame following the order of *x*, *y* and *z* (see Fig. 7), and $\varepsilon^*$ is the isotropic eigenstrain that is expressed as the difference of volumetric strain between inclusion and host assuming that they are not bounded by each other. The elliptic integrals $\psi$ and $\phi$ are expressed below:

$$\psi = \pi R^3 \int_\lambda^\infty \frac{1-\frac{R_1^2}{R^2+s}}{(R^2+s)^{\frac{3}{2}}} ds, \quad \text{(A3)}$$

where $\lambda = R_1^2 - R^2$ for host, $\lambda = 0$ for inclusion, and $R_1 = \sqrt{x_1^2 + x_2^2 + (x_3 - L)^2}$.

$$\phi = \pi R^3 \int_\lambda^\infty \frac{1-\frac{R_2^2}{R^2+s}}{(R^2+s)^{\frac{3}{2}}} ds, \quad \text{(A4)}$$

where $\lambda = R_2^2 - R^2$ for both host and inclusion, and $R_2 = \sqrt{x_1^2 + x_2^2 + (x_3 + L)^2}$. Here, we focus on the stress experienced by the inclusion and derive a simplified form for the pressure of inclusion. For the inclusion, the elliptic integrals are derived:

$$\psi = 2\pi\left(R^2 - \frac{1}{3}R_1^2\right), \quad \text{(A5)}$$

$$\phi = \frac{4}{3}\pi R^3 R_2^{-1}. \quad \text{(A6)}$$

The normal stresses in the inclusion are:

$$\sigma_{11} = \frac{\varepsilon^*(1+\nu)G}{2\pi(1-\nu)}\left[-4\pi - \frac{\partial^2\psi}{\partial x_1 x_1} + 4\nu\frac{\partial^2\phi}{\partial x_3 x_3} - (3-4\nu)\frac{\partial^2\phi}{\partial x_1 x_1} - 2x_3\frac{\partial^3\phi}{\partial x_3 x_1 x_1}\right]. \quad \text{(A7)}$$

$$\sigma_{22} = \frac{\varepsilon^*(1+\nu)G}{2\pi(1-\nu)}\left[-4\pi - \frac{\partial^2\psi}{\partial x_2 x_2} + 4\nu\frac{\partial^2\phi}{\partial x_3 x_3} - (3-4\nu)\frac{\partial^2\phi}{\partial x_2 x_2} - 2x_3\frac{\partial^3\phi}{\partial x_3 x_2 x_2}\right]. \quad \text{(A8)}$$

$$\sigma_{33} = \frac{\varepsilon^*(1+\nu)G}{2\pi(1-\nu)}\left[-4\pi - \frac{\partial^2\psi}{\partial x_3 x_3} + 4\nu\frac{\partial^2\phi}{\partial x_3 x_3} + (3-4\nu)\frac{\partial^2\phi}{\partial x_3 x_3} - 2x_3\frac{\partial^3\phi}{\partial x_3^3} - 2\frac{\partial^2\phi}{\partial x_3^2}\right]. \quad \text{(A9)}$$

By substituting $\psi$ and $\phi$ into the equations above, the normal stresses can be obtained. In deriving the pressure, i.e. negative mean stress, many terms in Eq. A7~A9 can be cancelled out. A simplified form is obtained as follow:

$$P_{\text{inc}} = \frac{4\varepsilon^*(1+\nu)G}{3(1-\nu)}\left[1 - \frac{2}{3}\frac{R^3}{R_2^3}(1+\nu)\left(\frac{3(z+L)^2}{R_2^2} - 1\right)\right]. \quad \text{(A10)}$$

The pre-factor $\frac{4\varepsilon^*(1+\nu)G}{3(1-\nu)}$ is in fact the initial pressure of the inclusion in infinite host loaded by the eigenstrain $\varepsilon^*$ under mechanical equilibrium. Therefore, we may simplify Eq. A10 as follows:

$$P_{\text{inc}} = P_{\text{ini}}[1 - \frac{2}{3}\frac{R^3}{R_2^3}(1+\nu)(\frac{3(z+L)^2}{R_2^2} - 1)]. \quad \text{(A11)}$$

where $P_{\text{ini}}$ is the inclusion pressure in infinite host loaded by eigenstrain $\varepsilon^*$ under mechanical equilibrium before moving it close to the thin-section surface. The equation can be nondimensionalized by using $R$ as length scale shown below:

$$\frac{P_{\text{inc}}}{P_{\text{ini}}} = 1 - \frac{2}{3}\frac{1+\nu}{\bar{R}_2^3}(\frac{3(\bar{z}+\bar{L})^2}{\bar{R}_2^2} - 1). \quad \text{(A12)}$$

The analytical solution for pressure in the mineral inclusion subject to an initial residual pressure $P_{\text{ini}}$ is obtained. When the inclusion is far from thin-section surface ($\bar{L} \to +\infty$, and $\bar{R}_2 \to +\infty$), the actual residual pressure approaches the expected

residual pressure based on classical elastic model ($P_{inc} \rightarrow P_{ini}$). Another potential application of the solution in Eq. A12 is for benchmarking numerical solutions. Due to the simplicity of the pressure expression, it is particularly suitable for quick validation of numerical models, e.g. finite-difference model presented in supplementary materials.

**References**


Aderogba, K., 1976. On eigenstresses in a semi-infinite solid. Math. Proc. Cambridge Philos. Soc. 80, 555–562. https://doi.org/10.1017/S0305004100053172

Angel, R.J., Alvaro, M., Miletich, R., Nestola, F., 2017a. A simple and generalised P–T–V EoS for continuous phase transitions, implemented in EosFit and applied to quartz. Contrib. to Mineral. Petrol. 172, 1–15. https://doi.org/10.1007/s00410-017-1349-x

Angel, R.J., Gonzalez-Platas, J., Alvaro, M., 2014. EosFit7c and a Fortran module (library) for equation of state calculations. Zeitschrift fur Krist. 229, 405–419. https://doi.org/10.1515/zkri-2013-1711

Angel, R.J., Mazzucchelli, M.L., Alvaro, M., Nestola, F., 2017b. EosFit-Pinc: A simple GUI for host-inclusion elastic thermobarometry. Am. Mineral. 102, 1957–1960. https://doi.org/10.2138/am-2017-6190

Angel, R.J., Nimis, P., Mazzucchelli, M.L., Alvaro, M., Nestola, F., 2015. How large are departures from lithostatic pressure? Constraints from host–inclusion elasticity. J. Metamorph. Geol. 33, 801–813. https://doi.org/10.1111/jmg.12138

Ashley, K.T., Caddick, M.J., Steele-MacInnis, M.J., Bodnar, R.J., Dragovic, B., 2014. Geothermobarometric history of subduction recorded by quartz inclusions in garnet. Geochemistry, Geophys. Geosystems 15, 350–360. https://doi.org/10.1002/2013GC005106

Bass, J.D., 1995. Elasticity of Minerals, Glasses, and Melts, in: Mineral Physics & Crystallography: A Handbook of Physical Constants. pp. 45–63. https://doi.org/10.1029/RF002p0045

Bayet, L., John, T., Agard, P., Gao, J., Li, J., 2018. Massive sediment accretion at ~ 80 km depth along the subduction interface :

Evidence from the southern Chinese Tianshan. Geology 46, 495–498.

Bonazzi, M., Tumiati, S., Thomas, J., Angel, R.J., Alvaro, M., 2019. Assessment of the reliability of elastic geobarometry with quartz inclusions. Lithos 350–351, 105201. https://doi.org/10.1016/j.lithos.2019.105201

Campomenosi, N., Mazzucchelli, M.L., Mihailova, B.D., Scambelluri, M., Angel, R.J., Nestola, F., Reali, A., Alvaro, M., 2018. How geometry and anisotropy affect residual strain in host inclusion system: coupling experimental and numerical approaches. Am. Mineral. 103, 2032–2035. https://doi.org/10.1111/ijlh.12426

Castro, A.E., Spear, F.S., 2017. Reaction overstepping and re-evaluation of peak P–T conditions of the blueschist unit Sifnos, Greece: implications for the Cyclades subduction zone. Int. Geol. Rev. 59, 548–562. https://doi.org/10.1080/00206814.2016.1200499

Chen, J., Wang, Q., Zhai, M., Ye, K., 1996. Plastic deformation of garnet in eclogite. Sci. China 39, 18–25.

Dabrowski, M., Powell, R., Podladchikov, Y., 2015. Viscous relaxation of grain-scale pressure variations. J. Metamorph. Geol. 33, 859–868. https://doi.org/10.1111/jmg.12142

Dekker, E.H.L.J., Rieck, G.D., 1974. Microhardness investigations on manganese aluminate spinels. J. Mater. Sci. 9, 1839–1846.

Enami, M., Nishiyama, T., Mouri, T., 2007. Laser Raman microspectrometry of metamorphic quartz: A simple method for comparison of metamorphic pressures. Am. Mineral. 92, 1303–1315. https://doi.org/10.2138/am.2007.2438

Evans, B., Goetze, C., 1979. The temperature variation of hardness of olivine and its implication for polycrystalline yield stress. J. Geophys. Res. 84, 5505–5524. https://doi.org/10.1029/JB084iB10p05505

Farber, K., Caddick, M.J., John, T., 2014. Controls on solid-phase inclusion during porphyroblast growth: insights from the Barrovian sequence (Scottish Dalradian). Contrib. to Mineral. Petrol. 168, 1089. https://doi.org/10.1007/s00410-014-1089-0

Ferrero, S., Angel, R.J., 2018. Micropetrology: Are inclusions grains of truth? J. Petrol. 59, 1671–1700. https://doi.org/10.1093/petrology/egy075

Gerya, T. V., 2010. Introduction to Numerical Geodynamic Modelling. Cambridge University Press.

Gillet, P., Ingrin, J., Chopin, C., 1984. Coesite in subducted continental crust : P - T history deduced from an elastic model. Earth Planet. Sci. Lett. 70, 426–436.

Gréaux, S., Yamada, A., 2014. P-V-T equation of state of Mn3Al2Si3O12 spessartine garnet. Phys. Chem. Miner. 41, 141–149. https://doi.org/10.1007/s00269-013-0632-2

Guiraud, M., Powell, R., 2006. P-V-T relationships and mineral equilibria in inclusions in minerals. Earth Planet. Sci. Lett. 244, 683–694. https://doi.org/10.1016/j.epsl.2006.02.021

Izraeli, E.S., Harris, J.W., Navon, O., 1999. Raman barometry of diamond formation 173, 351–360.

Jasiuk, I., Tsuchida, E., Mura, T., 1991. Spheroidal sliding inclusion in an elastic half-space. Appl. Mech. Rev. 44, S143–S149. https://doi.org/10.1115/1.3121346

Kachanov, L.A., 1971. Foundations of the Theory of Platicity. North-Holland Publishing Company.

Karato, S., Wang, Z., Liu, B., Fujino, K., 1995. Plastic deformation of garnet: systematics and implications for the rheology of the mantle transition zone. Earth Planet. Sci. Lett. 130, 13–20.

Kohn, M.J., 2014. "Thermoba-Raman-try": Calibration of spectroscopic barometers and thermometers for mineral inclusions. Earth Planet. Sci. Lett. 388, 187–196. https://doi.org/10.1016/j.epsl.2013.11.054

Korsakov, A. V., Perrakim, M., Zhukov, V.P., De Gussem, K., Vandenabeele, P., Tomilenko, A.A., 2009. Is quartz a potential indicator of ultrahigh-pressure metamorphism ? Laser Raman spectroscopy of quartz inclusions in ultrahigh-pressure garnets. Eur. J. Mineral. 21, 1313–1323. https://doi.org/10.1127/0935-1221/2009/0021-2006

Kouketsu, Y., Hattori, K., Guillot, S., Rayner, N., 2016. Eocene to Oligocene retrogression and recrystallization of the Stak eclogite in northwest Himalaya. Lithos 240–243, 155–166. https://doi.org/10.1016/j.lithos.2015.10.022

Liu, L., Mernagh, T.P., 1992. High Pressure Raman study of the a-quartz forms of SiO2 and GeO2 at room temperature. High Temp. Press. 24, 13–21.

Mazzucchelli, M.L., Burnley, P., Angel, R.J., Morganti, S., Domeneghetti, M.C., Nestola, F., Alvaro, M., 2018. Elastic geothermobarometry: Corrections for the geometry of the host-inclusion system. Geology 1–4.

Milani, S., Nestola, F., Alvaro, M., Pasqual, D., Mazzucchelli, M.L., Domeneghetti, M.C., Geiger, C.A., 2015. Diamond-garnet geobarometry: The role of garnet compressibility and expansivity. Lithos 227, 140–147. https://doi.org/10.1016/j.lithos.2015.03.017

Mindlin, R.D., Cheng, D.H., 1950. Thermoelastic Stress in the Semi-Infinite Solid. J. Appl. Phys. 931, 931–933. https://doi.org/10.1063/1.1699786

Moulas, E., Schmalholz, S.M., Podladchikov, Y., Tajčmanová, L., Kostopoulos, D., Baumgartner, L., 2019. Relation between mean stress, thermodynamic, and lithostatic pressure. J. Metamorph. Geol. 37, 1–14. https://doi.org/10.1111/jmg.12446

Murri, M., Mazzucchelli, M.L., Campomenosi, N., Korsakov, A. V., Prencipe, M., Mihailova, B.D., Scambelluri, M., Angel, R.J., Alvaro, M., 2018. Raman elastic geobarometry for anisotropic mineral inclusions. Am. Mineral.

Reiner, M., 1964. The Deborah Number. Phys. Today 17, 62–62.

Rosenfeld, J.L., Chase, A.B., 1961. Pressure and temperature of crystallization from elastic effects around solid inclusions in minerals? Am. J. Sci. https://doi.org/10.2475/ajs.259.7.519

Schmidt, C., Ziemann, M.A., 2000. In situ Raman spectroscopy of quartz: A pressure sensor for hydrothermal diamond-anvil cell experiments at elevated temperatures. Am. Mineral. 85, 1725–1734.

Seo, K., Mura, T., 1979. The elastic field in a half space due to ellipsoidal inclusions with uniform dilatational eigenstrains. J. Appl. Mech. 46, 568–572. https://doi.org/10.1115/1.3424607

Smedskjaer, M.M., Jensen, M., Yue, Y.Z., 2008. Theoretical calculation and measurement of the hardness of diopside. J. Am. Ceram. Soc. 91, 514–518. https://doi.org/10.1111/j.1551-2916.2007.02166.x

Spear, F.S., Thomas, J.B., Hallett, B.W., 2014. Overstepping the garnet isograd : a comparison of QuiG barometry and thermodynamic modeling. Contrib. to Mineral. Petrol. 168, 1059. https://doi.org/10.1007/s00410-014-1059-6

Taguchi, T., Enami, M., Kouketsu, Y., 2019a. Metamorphic record of the Asemi-gawa eclogite unit in the Sanbagawa belt,

southwest Japan: Constraints from inclusions study in garnet porphyroblasts. J. Metamorph. Geol. 37, 181–201. https://doi.org/10.1111/jmg.12456

Taguchi, T., Igami, Y., Miyake, A., Enami, M., 2019b. Factors affecting preservation of coesite in ultrahigh-pressure metamorphic rocks: Insights from TEM observations of dislocations within kyanite. J. Metamorph. Geol. 37, 401–414. https://doi.org/10.1111/jmg.12470

Tajčmanová, L., Podladchikov, Y., Powell, R., Moulas, E., Vrijmoed, J.C., Connolly, J.A.D., 2014. Grain-scale pressure variations and chemical equilibrium in high-grade metamorphic rocks. J. Metamorph. Geol. 32, 195–207. https://doi.org/10.1111/jmg.12066

Thomas, J.B., Spear, F.S., 2018. Experimental study of quartz inclusions in garnet at pressures up to 3.0 GPa: evaluating validity of the quartz-in-garnet inclusion elastic thermobarometer. Contrib. to Mineral. Petrol. 173, 1–14. https://doi.org/10.1007/s00410-018-1469-y

Tsuchida, E., Nakahara, I., 1970. Three dimensional stress concentration around a spherical cavity in a semi infinite elastic body. Bull. Jpn. Soc. Mech 13, 499–508. https://doi.org/https://doi.org/10.1299/jsme1958.13.499

Van Der Molen, I., Van Roermund, H.L.., 1986. The pressure path of solid inclusions in minerals : the retention of coesite inclusions during uplift. Lithos 19, 317–324.

Vermeer, P.A., De Borst, R., 1984. Non-associated plasticity for soils, concrete and rock, in: Physics of Dry Granular Media. NATO ASI Series, pp. 163–196.

Walters, J.B., Kohn, M.J., 2014. Examining the temperature range suitable for Quartz-in-Garnet Geoba-Raman-try, in: 11th International GeoRaman Conference. p. 5023.

Wang, Z., Ji, S., 1999. Deformation of silicate garnets: Brittle-ductile transition and its geological implications. Can. Mineral. 37, 525–541.

Whitney, D.L., Broz, M., Cook, R.F., 2007. Hardness, toughness, and modulus of some common metamorphic minerals. Am. Mineral. 92, 281–288. https://doi.org/10.2138/am.2007.2212

Whitney, D.L., Cooke, M.L., Du Frane, S.A., 2000. Modeling of radial microcracks at corners of inclusions in garnet using fracture mechanics. J. Geophys. Res. 105, 2843. https://doi.org/10.1029/1999JB900375

Wolfe, O.M., Spear, F.S., 2017. Determining the amount of overstepping required to nucleate garnet during Barrovian regional metamorphism, Connecticut Valley Synclinorium. J. Metamorph. Geol. 36, 79–94. https://doi.org/10.1111/ijlh.12426

Wong, T.Y., Bradt, R.C., 1992. Microhardness anisotropy of single crystals of calcite, dolomite and magnesite on their cleavage planes. Mater. Chem. Phys. 30, 261–266. https://doi.org/10.1016/0254-0584(92)90234-Y

Yamamoto, J., Kagi, H., Kaneoka, I., Lai, Y., Prikhod'ko, V.S., Arai, S., 2002. Fossil pressures of fluid inclusions in mantle xenoliths exhibiting rheology of mantle minerals: Implications for the geobarometry of mantle minerals using micro-Raman spectroscopy. Earth Planet. Sci. Lett. 198, 511–519. https://doi.org/10.1016/S0012-821X(02)00528-9

Yardley, B.W.., Bodnar, R.J., 2014. Fluids in the Upper Continental Crust. Front. Geofluids 3, 1–127. https://doi.org/10.1002/9781444394900.ch17

Yuan, X., Liu, X., Wang, L., Lu, X., 2017. Density and hardness of Nd-doped zircon ceramics as nuclear waste forms. IOP Conf. Ser. Earth Environ. Sci. 61. https://doi.org/10.1088/1755-1315/61/1/012140

Zhang, Y., 1998. Mechanical and phase equilibria in inclusion-host systems. Earth Planet. Sci. Lett. 157, 209–222. https://doi.org/10.1016/S0012-821X(98)00036-3

Zhong, X., Andersen, N.H., Dabrowski, M., Jamtviet, B., 2019. Zircon and quartz inclusions in garnet used for complimentary Raman- thermobarometry: application to the Holsnøy eclogite, Bergen Arcs, Western Norway. Contrib. to Mineral. Petrol. 4, 1–17. https://doi.org/10.1007/s00410-019-1584-4

Zhong, X., Dabrowski, M., Jamtveit, B., 2018a. Analytical solution for the stress field in elastic half space with a spherical pressurized cavity or inclusion containing eigenstrain. Geophys. J. Int. 216, 1100–1115.

Zhong, X., Moulas, E., Tajčmanová, L., 2018b. Tiny timekeepers witnessing high-rate exhumation processes. Sci. Rep. 8, 2234. https://doi.org/10.1038/s41598-018-20291-7

**Table**

**Table 1**. Averaged ~~cohesion~~plastic strength from microhardness tests for some minerals at room conditions. ~~Cohesion~~Strength is converted from microhardness based on $C_h = H/C_g$, where the geometry constant $C_g$ is taken as 3. Raw data are dependent on crystallographic orientation, composition and applied load that are examined in some of the involved references.

| Minerals | ~~Cohesion~~Yield |
|---|---|
| calcite[2] | 0.6 |
| zircon[4] | 1.2 |
| dolomite[2] | 1.5 |
| orthoclase[1] | 2.3 |
| andalusite[1] | 2.3 |
| diopside[3] | 2.7 |
| sillimanite[1] | 3.7 |
| quartz[1] | 4.0 |
| kyanite[1] | 4.0 |
| spinel[5] | 4.1 |
| grossular[1] | 4.4 |
| almandine-pyrope[1] | 5.0 |

[1]Data reported in Whitney et al. (2007).

[2]Data reported in Wong and Bradt (1992). The reported data for calcite and dolomite are averaged from the applied load and azimuthal angle from $[10\bar{1}\bar{1}]$.

[3]Data reported in Smedskjaer et al. (2008).

[4]Data reported in Yuan et al. (2017)

[5]Data reported in Dekker and Rieck (1974). The reported data are averaged from the applied load at [110] and [100].

**Figures**

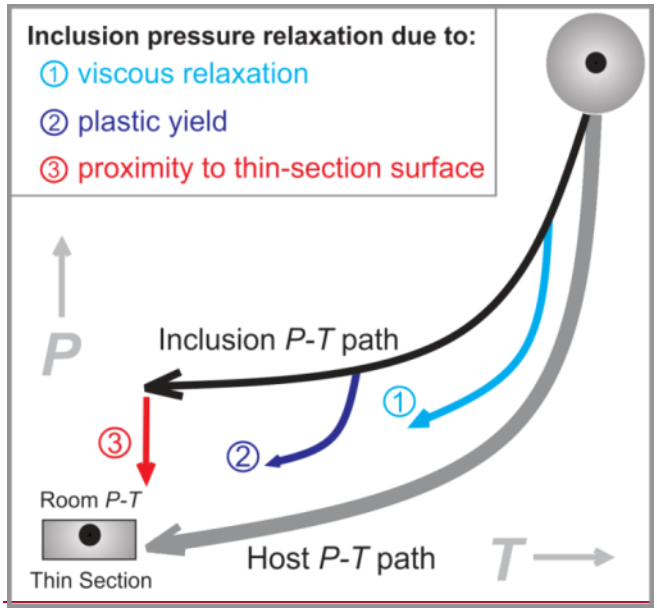
Inclusion pressure relaxation due to:
① viscous relaxation
② plastic yield
③ proximity to thin-section surface
P
Inclusion P-T path
①
②
③
Room P-T
Thin Section
Host P-T path
T

655

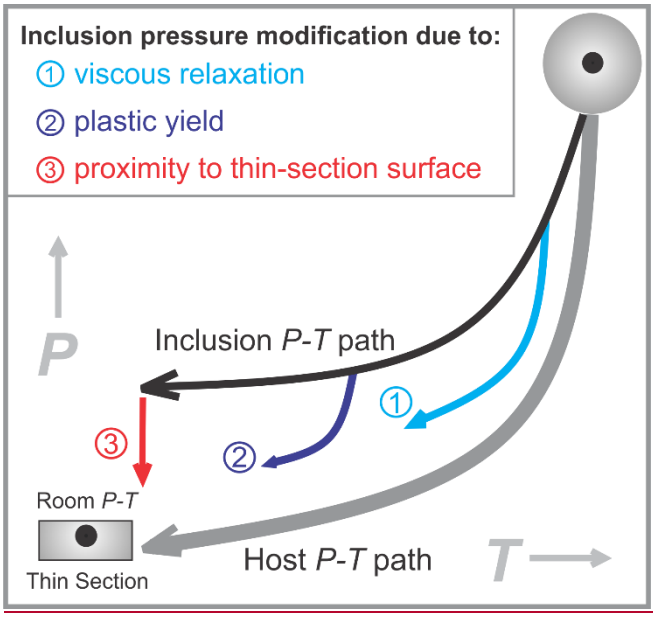
Inclusion pressure modification due to:
① viscous relaxation
② plastic yield
③ proximity to thin-section surface
P
Inclusion P-T path
①
②
③
Room P-T
Thin Section
Host P-T path
T

Fig. 1. Schematic illustration for the residual pressure ~~development and relaxation.~~. The grey and black curves are retrograde *P*-*T* paths for host and inclusion, respectively. Pressure ~~relaxation~~drop is possibly due to following reasons: 1) viscous relaxation preferentially occurs at high temperature conditions; 2) plastic yield commonly occurs at low confining pressures where residual pressure is high; 3) thin-section preparation that drives inclusion close to thin-section surface. Note that this illustration refers to systems where the inclusion is elastically softer than its host (e.g. quartz in garnet).

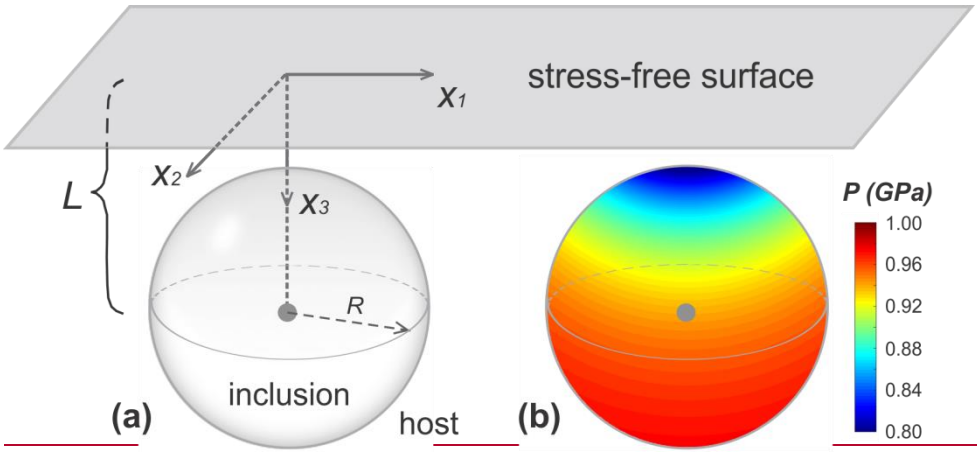


665

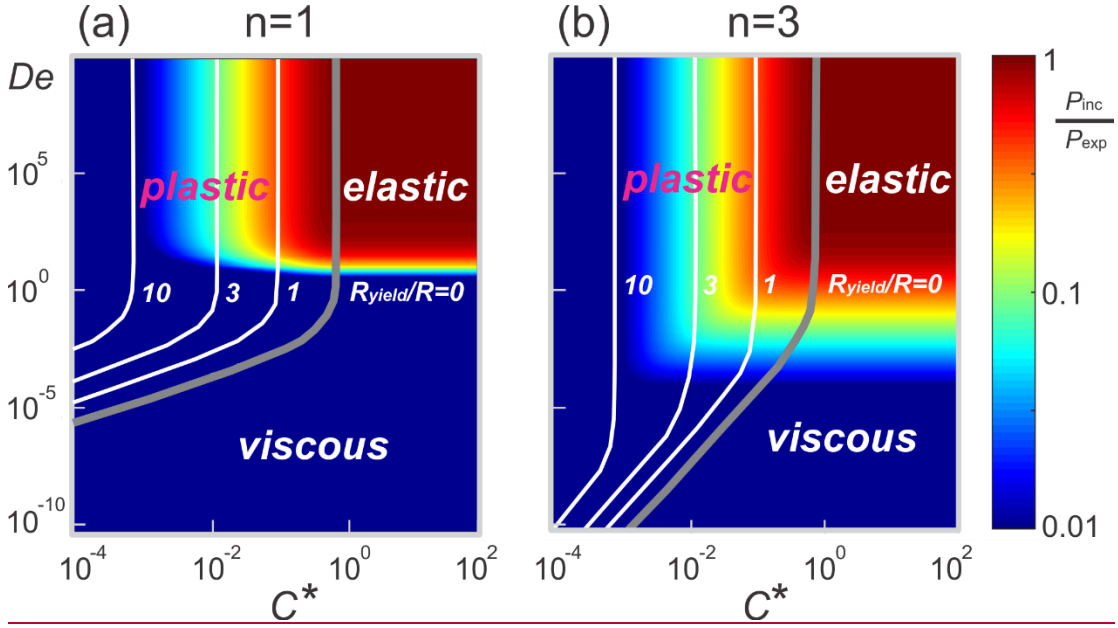


Fig. 2. **A:** Model configuration of mineral inclusion close to thin-section surface. The distance between the surface to inclusion centre is denoted by $L$. **B:** Pressure distribution on $x$-$z$ plane ($L = 1.5R$). Initially the inclusion contains 1GPa residual pressure and is relaxed when brought next to the stress-free surface. The analytical solution of Eq. 32 is used for the pressure plot.

670

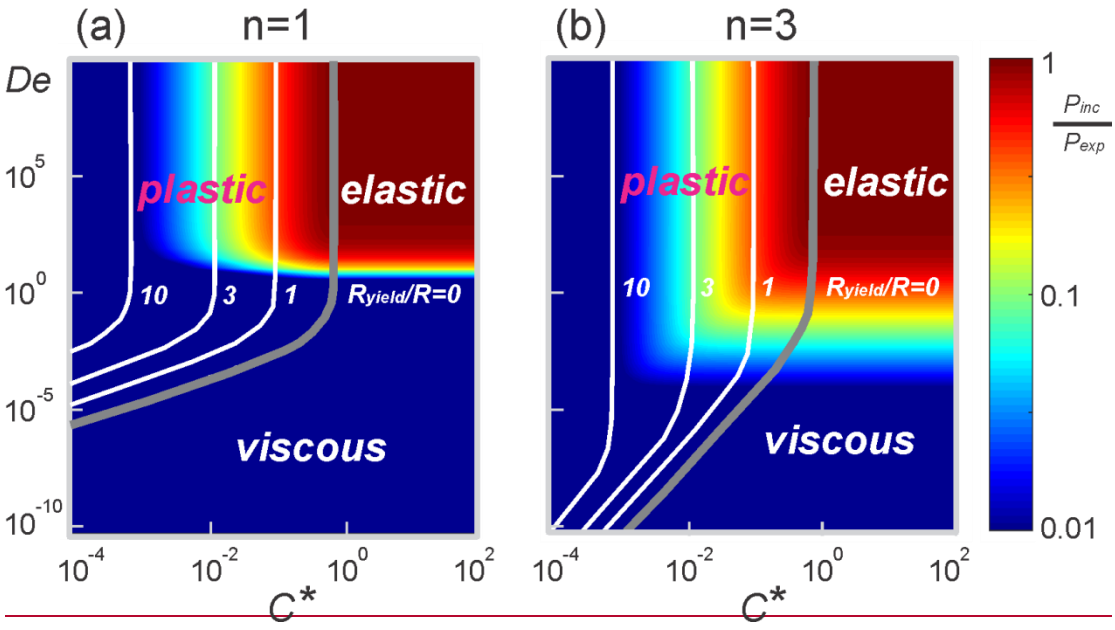


~~Fig. 3.~~ Inclusion pressure as a function of Deborah number and ~~Cohesion number~~dimensionless yield strength given different stress exponents. The contours denote the radius of plastic yield region $R_{yield}$ scaled by inclusion radius. The thick grey contour represents the onset of plastic yield. Three regimes are labelled: 1) elastic ($De > 1$, $C^* > 1$); 2) viscous ($De < 1$ and $C^*$ is above the onset of plastic yield); 3) plastic ($C^* < 1$, $De$ is above the onset of plastic yield). To obtain the results, a residual pressure is prescribed at the beginning and the confining pressure and temperature are fixed, i.e. no temporal variations of *P*-*T* conditions.

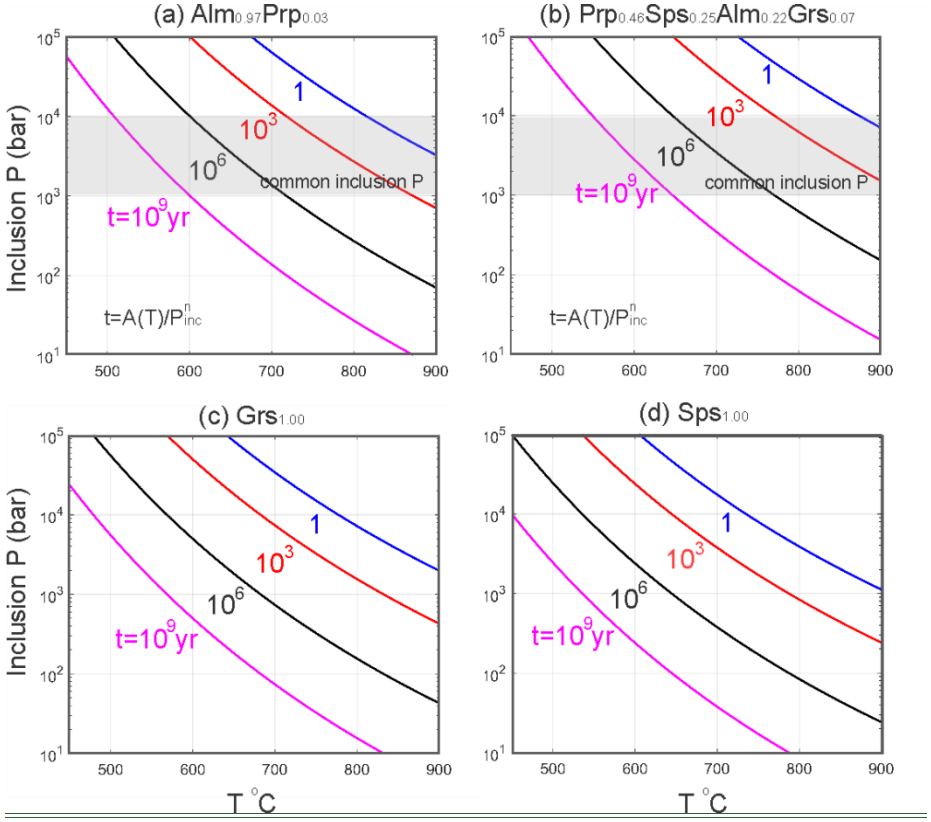
(a) Alm0.97Prp0.03
(b) Prp0.46Sps0.25Alm0.22Grs0.07
(c) Grs1.00
(d) Sps1.00
Inclusion P (bar)
T °C
1
10^3
10^6
t=10^9yr
common inclusion P
t=A(T)/P^n_inc

680

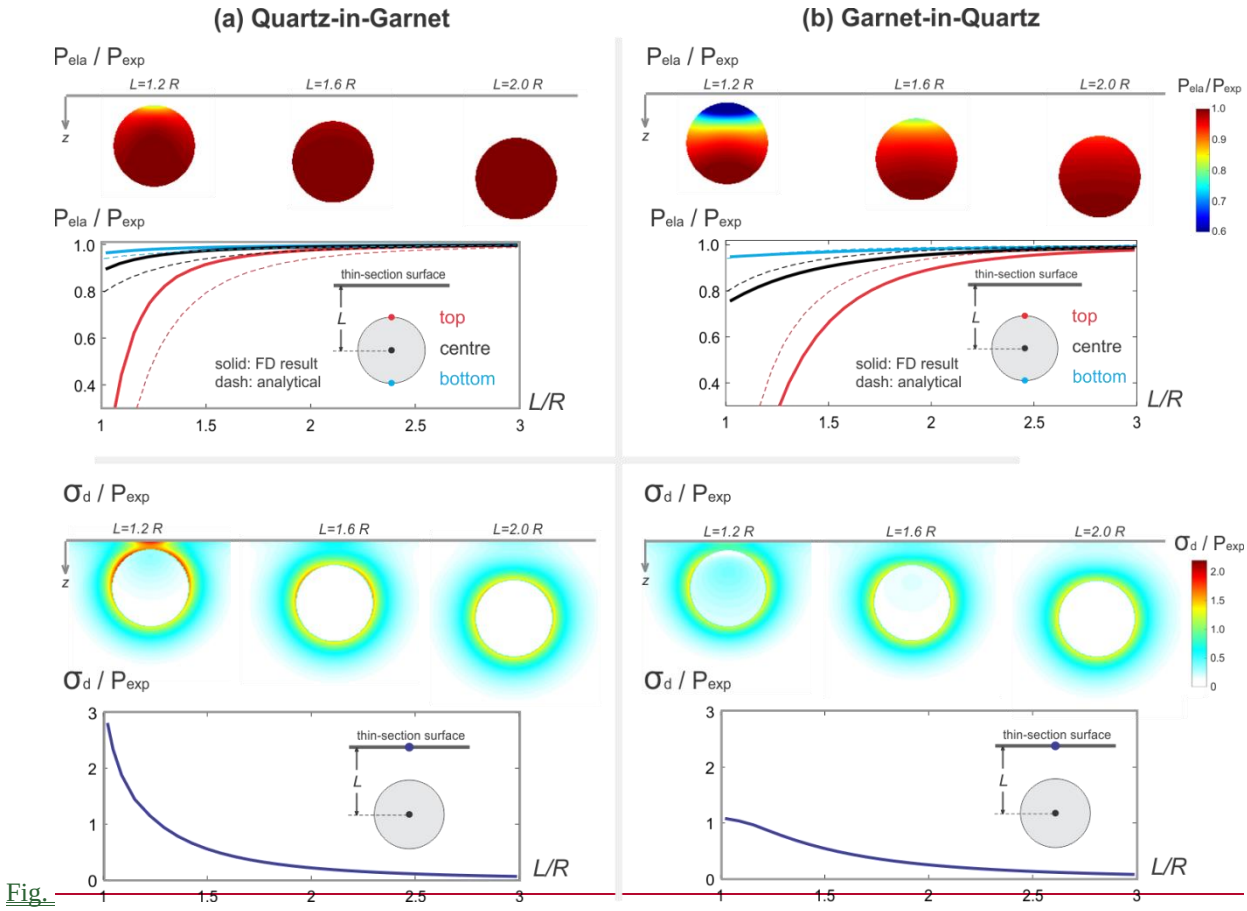


Fig.

~~Fig. 4. Dimensionless pressure and differential stress plotted on *x*-*z* plane, or as a function of dimensionless depth. **A:** Quartz-in-pyrope system; **B**: Pyrope-in-quartz system. 3For the profiles, pressure and differential stress are measured at different locations denoted by the coloured dots. In the top panel, the dashed curves in the pressure plot are based on the analytical solution in Eq. 32 considering the same elastic moduli between inclusion and host, while the solid curves are based on finite difference results. The discrepancy between the solid (numerical solution) and dashed (analytical solution) curves in **A** is due to the fact that the host elasticity is different than the inclusion.~~

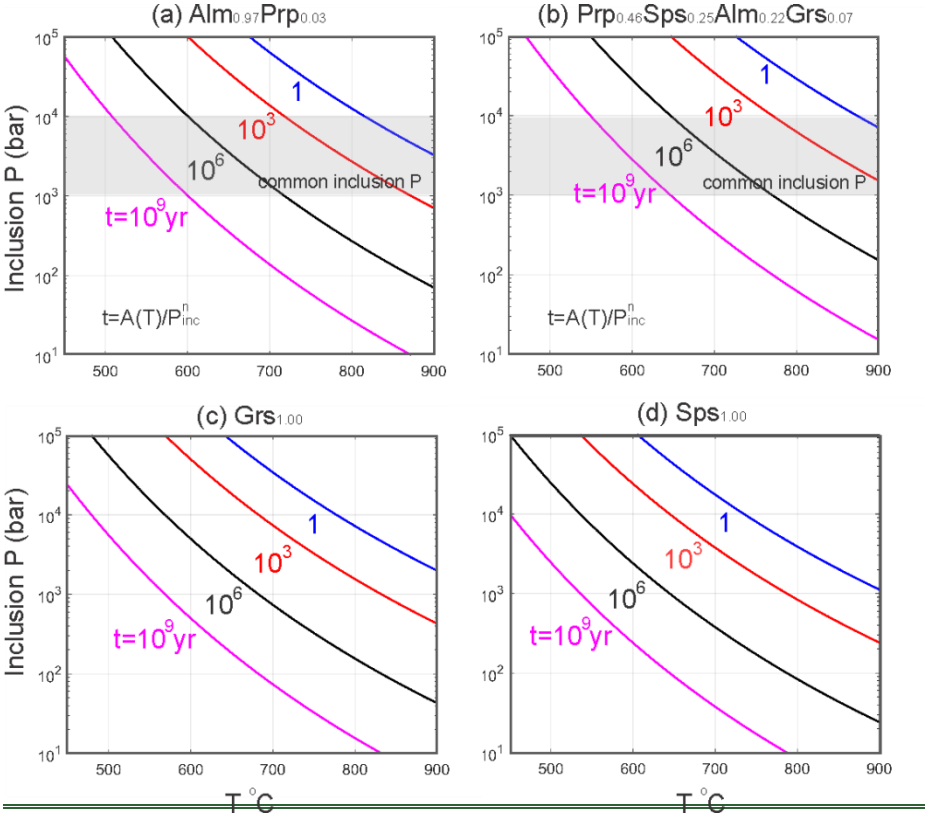


~~Fig. 5~~. Viscous relaxation time (in years) of different garnet host as functions of temperature and inclusion overpressure. The viscous relaxation time is calculated based on the expression of Deborah number (*De*=1) in Eq. 19~~18~~. The ~~viscous~~viscosity's pre-factor ~~(A)~~ is *T* dependent and is obtained using the flow law from Wang and Ji (1999). The melting temperature is from Karato et al. (1995) (the melting temperature of almost pure almandine is taken from the data of Mohawk Garnet Inc. to be 1588K). Shear modulus is from Bass (1995). ~~Viscosity pre-factor $A$ is calculated as: $\frac{G^n}{2B}\exp(\frac{g \cdot T_m}{T})$, where $B = \exp(40.1)$ in $s^{-1}$, $g = 32$ and the stress exponent $n=3$~~The flow law is given in the main text (Wang and Ji, 1999). The four garnet endmembers are almandine (Alm), grossular (Grs), pyrope (Prp) and spessartine (Sps).

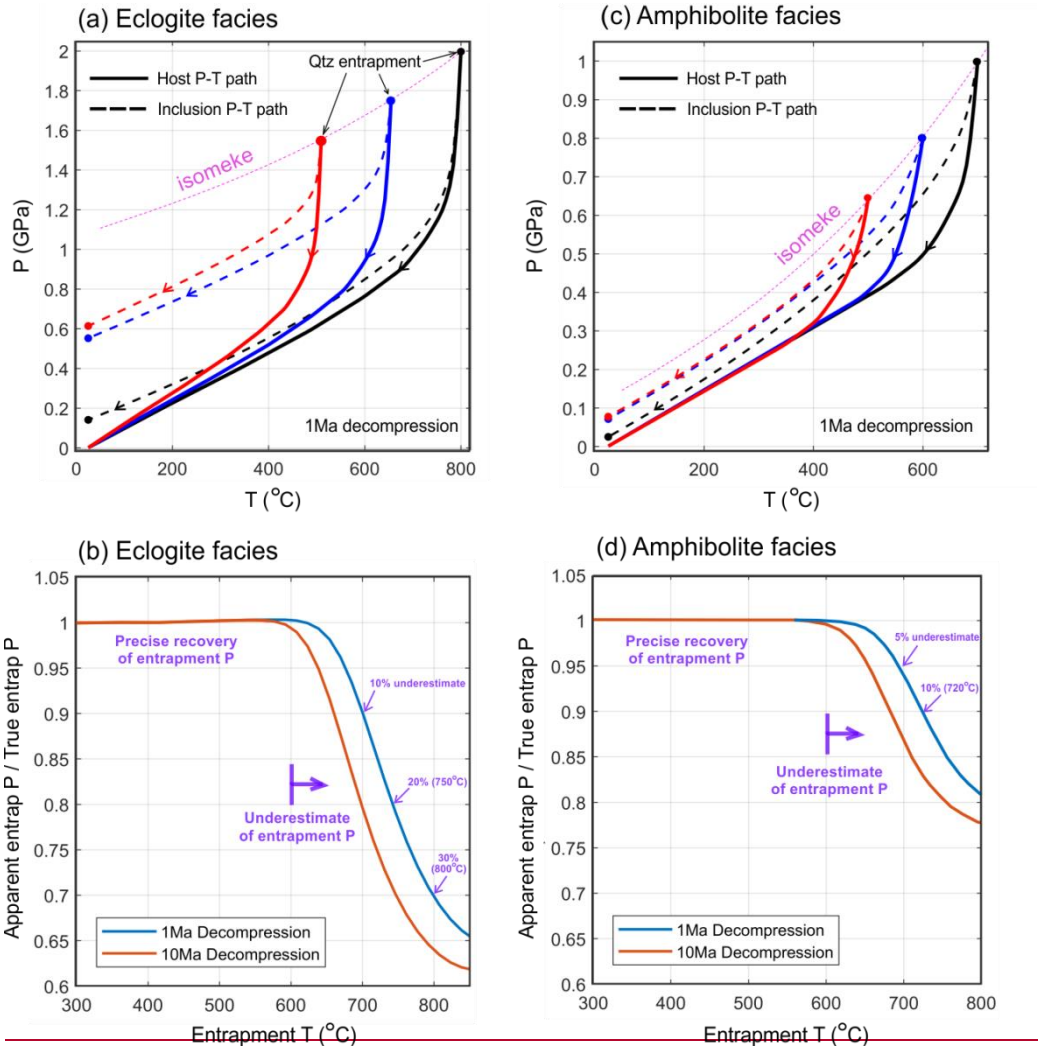
(a) Eclogite facies
Host P-T path
Inclusion P-T path
Qtz entrapment
isomeke
1Ma decompression
P (GPa)
T (°C)
(c) Amphibolite facies
Host P-T path
Inclusion P-T path
isomeke
1Ma decompression
P (GPa)
T (°C)
(b) Eclogite facies
Precise recovery of entrapment P
10% underestimate
20% (750°C)
30% (800°C)
Underestimate of entrapment P
1Ma Decompression
10Ma Decompression
Apparent entrap P / True entrap P
Entrapment T (°C)
(d) Amphibolite facies
Precise recovery of entrapment P
5% underestimate
10% (720°C)
Underestimate of entrapment P
1Ma Decompression
10Ma Decompression
Apparent entrap P / True entrap P
Entrapment T (°C)

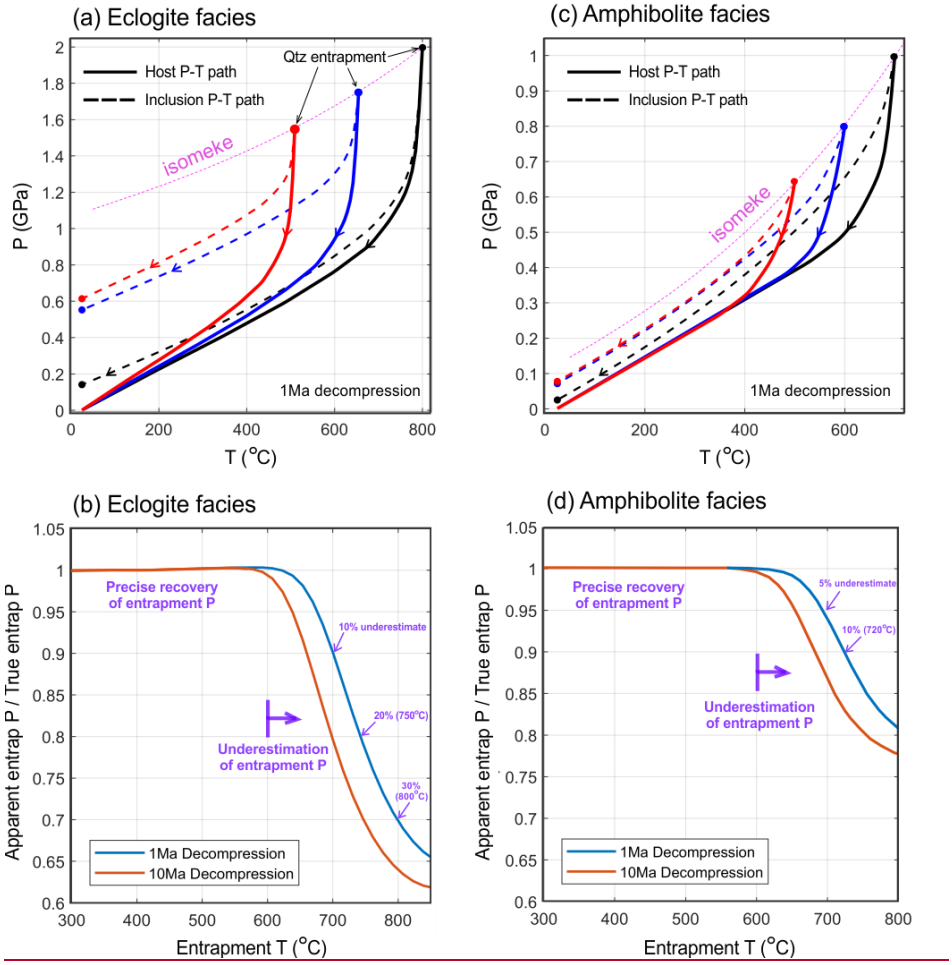


Fig. ~~6. A.~~4. **(a)** Synthetic retrograde *P-T* paths from eclogite facies metamorphic conditions. The quartz inclusions are entrapped within almandine at different peak *P-T* conditions along the same isomeke~~.~~, thus a purely-elastic model would predict the same value for the residual inclusion P. Due to viscous relaxation, the residual *P* is lower than the pressure predicted by an elastic model. In ~~B.~~**(b)**, the apparent entrapment *P* is calculated based on the relaxed residual inclusion pressure given different entrapment *T* along the elastic isomeke that is given in ~~A.~~**(a)**. Pressure relaxation is manifested by lower values of apparent entrapment *P* and it becomes more significant if the host experiences high temperatures with time. ~~C~~**(c)** and ~~D~~**(d)** are the same plots for amphibolite-facies entrapment conditions. The amount of viscous relaxation is less compared to eclogite facies due to the lower magnitude of inclusion overpressure and the stress dependent viscosity of garnet host. Pure almandine garnet is used as host and its flow law is from Wang and Ji (1999).

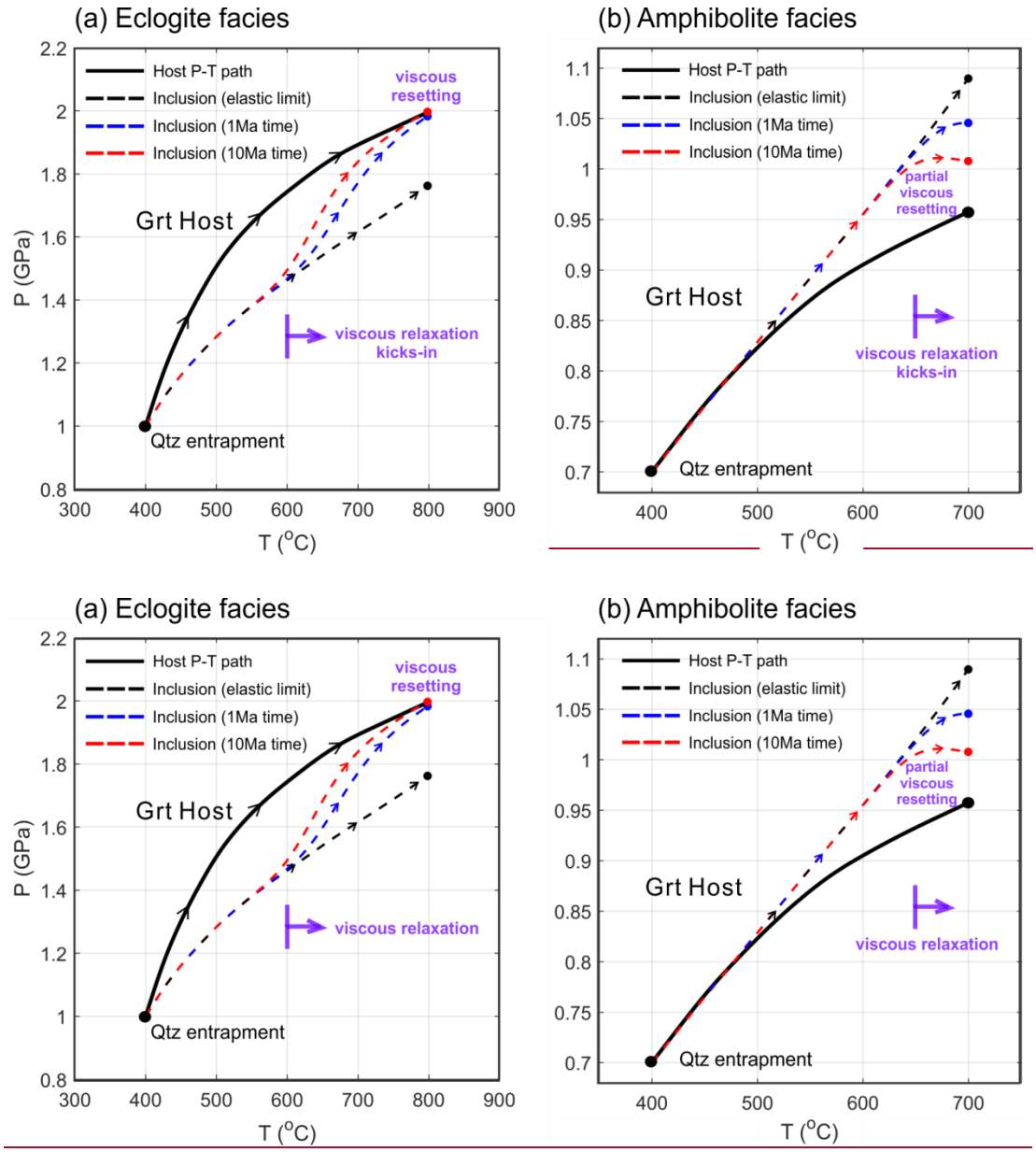


710 Fig. ~~7~~5. Prograde *P-T* path for inclusion (dashed curve) and host (solid curve). ~~A~~**(a)** is for rocks that experienced eclogite-facies peak *P-T* conditions. The quartz inclusion is entrapped at 400 °C and 1 GPa. Along the given prograde *P-T* path, viscous relaxation becomes significant at >600 °C. The duration of prograde *P-T* path is illustrated with different colour (1 Ma and 10 Ma, see legend). At 800 °C, the quartz inclusion pressure is reset to the confining pressure (host). For rocks that experienced

amphibolite-facies peak *P-T* conditions~~;~~ **(b),** viscous relaxation becomes significant at ca. 650~700 °C and the quartz inclusion pressure is partially reset at 700 °C. Pure almandine garnet is used as host and its flow law is from Wang and Ji (1999).

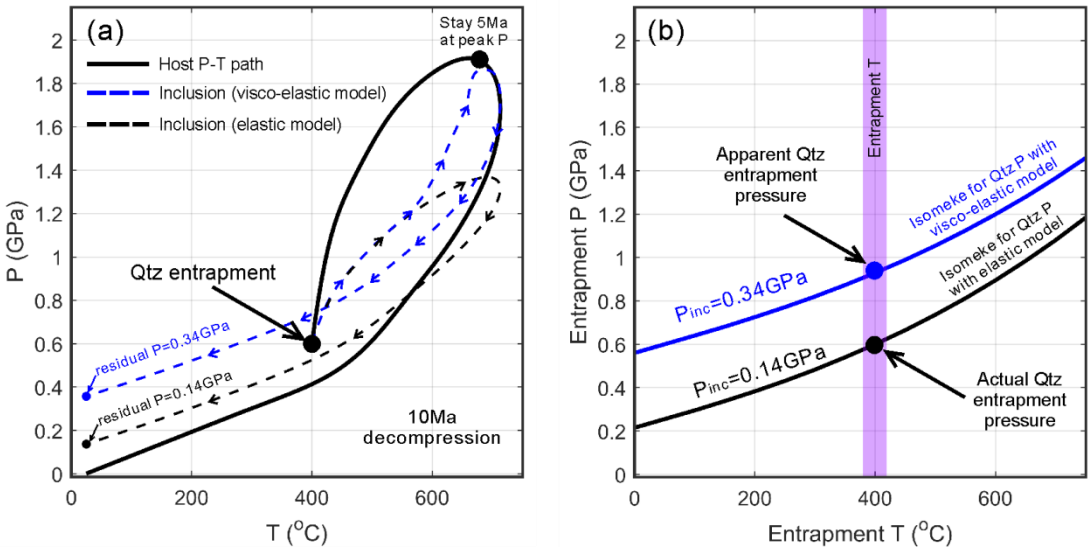


Fig. ~~8. A.~~6. **(a)** Clockwise *P-T* path of inclusion (dashed curve) and host (solid curve). The dashed black curve shows the inclusion *P-T* path based on pure elastic model and the blue dashed curve is based on visco-elastic model. The quartz inclusion is entrapped into almandine garnet at 400 °C, 0.6 GPa. The prograde *P-T* path lasts 5 Ma, and the rock stays at peak *P* for 5 Ma before retrograde *P-T* path, which lasts 10 Ma. The residual pressure preserved by the quartz inclusion that was subject to viscous relaxation is in fact higher than the elastic limit. Therefore, ~~its~~the apparent entrapment pressure, calculated using elastic isomeke ~~becomes~~, is higher than the actual entrapment pressure as shown in ~~B.~~**(b).** This may lead to ca. 3~4 kbar apparent overstepping effect. The almandine flow law is from Wang and Ji (1999).

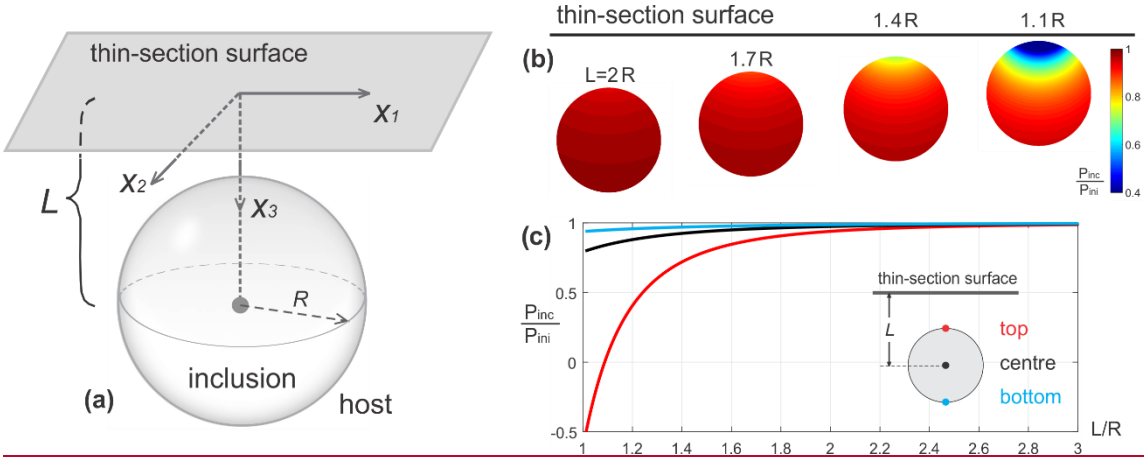


Fig. 7. **(a)** Analytical model configuration of a mineral inclusion close to the thin-section surface. The distance between the surface to inclusion centre is denoted by $L$. **(b)** Pressure distribution on $x$-$z$ plane. The pressure is scaled by the initial inclusion pressure ($P_{ini}$). The initial inclusion pressure is under force equilibrium in infinite host. The analytical model describes the amount of pressure release when the inclusion approaches the thin-section surface. **(c)** Pressure at three localities (inclusion top, centre and bottom) as a function of dimensionless depth $L/R$. The analytical solution of Eq. 22 is used for the pressure plot.

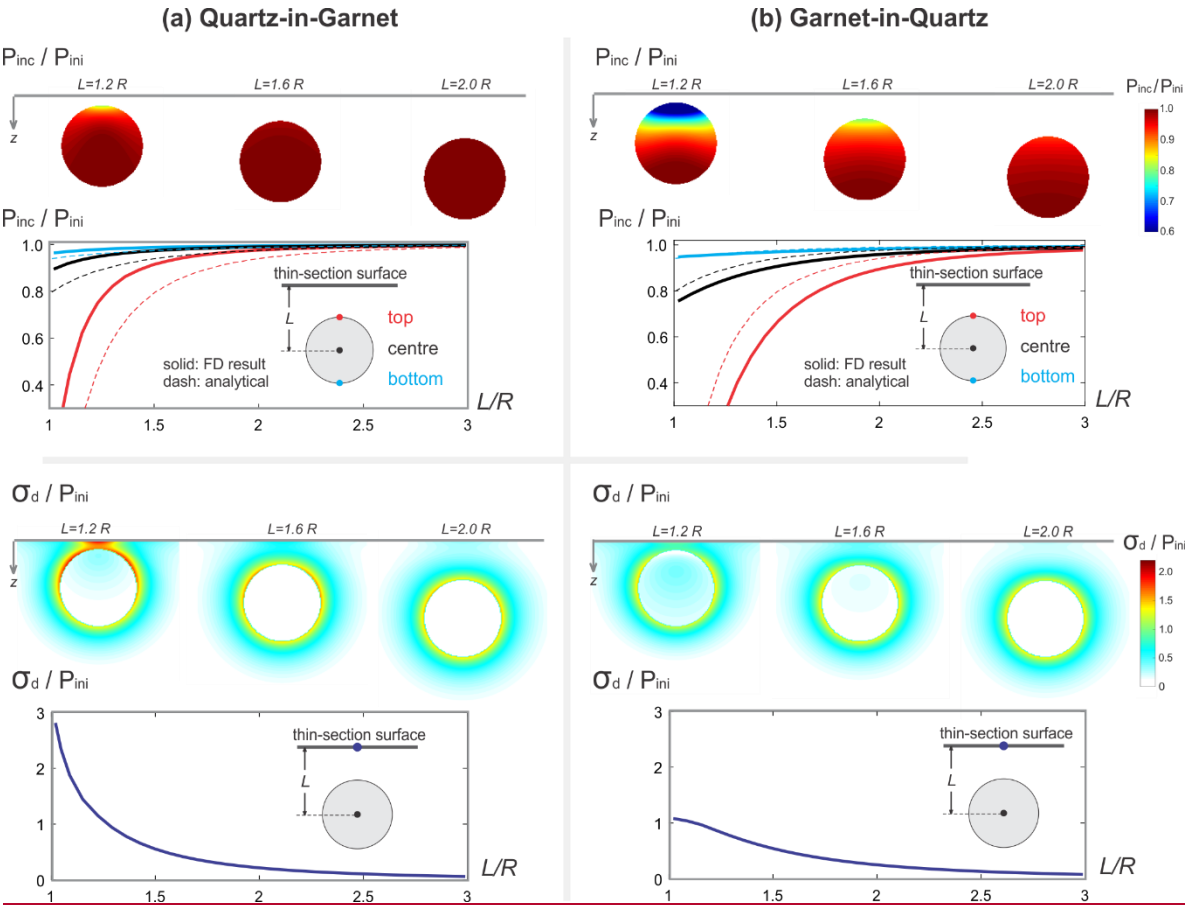


Fig. 8. Dimensionless pressure and differential stress plotted on *x*-*z* plane, or as a function of dimensionless depth. **(a)** Quartz-in-pyrope system; **(b)** Pyrope-in-quartz system. For the profiles, pressure and differential stress are measured at different locations denoted by the coloured dots. In the top panel, the dashed curves in the pressure plot are based on the analytical solution in Eq. 22 considering the same elastic moduli between inclusion and host, while the solid curves are based on finite difference results. The discrepancy between the solid (numerical solution) and dashed (analytical solution) curves in **(a)** is due to the fact that the host elasticity is different than the inclusion.

***General reply to reviewer 1***

*We thank the reviewer for the very careful examination of our work and helpful comments that have greatly improved the quality of our paper. All the comments from the reviewer have been carefully considered and point-by-point replies have been provided in this letter. The original comments from the reviewer are in "*regular black*" and our replies are in "italic blue".*

Comments from Reviewer 1

Presented manuscript discusses pressure variations around inclusions in the homogeneous rock matrix and their implications for the accuracy of Raman-thermobarometry measurements. Authors study two different processes that might lead to stress changes around a single inclusion: stress relaxation on a geological time scale due to visco-plastic stress relaxation and proximity of the free surface to the mineral inclusion during sample preparation in the lab. Authors show that both stress relaxation and presence of free surface might alter stresses inside inclusion and in the host matrix. Hence, they might lead to erroneous estimations during Raman-thermobarometry.

While this is an interesting paper, its logic and presentation could be improved. Authors are using two different problem setups and switch in the text from one of them to another without much mentioning of it. I would recommend revising the manuscript and clearly separate results related to sample preparation (i.e., setup with elastic solution for half-space) and results related to stress relaxation on a geological time scale.

*This is a very helpful comment. Indeed, our previous structure mix the two main parts of the model.*

*We have re-structured the entire manuscript to clearly separate the two different models and corresponding results/discussions. We hope our revised structure will be clearer for readers.*

Throughout the manuscript, use of term "relaxation" with respect to changes in stress due to the presence of free boundary as in sample preparation setup and due to plastic effects is incorrect and confusing. See e.g. original paper by Zhang (1998) where he states that "Plastic yielding does not relax the stress but does limit the deviatoric stress". I would call these processes rather "stress release". Besides, authors consider visco-elasto-plastic model for stress relaxation where plasticity contributes simultaneously with viscosity, i.e. purely plastic (or elastoplastic) stress release is not considered.

*We agree with the reviewer's comment and we have followed the reviewer's suggestion to change "stress relaxation" in plastic yield situation and proximity to surface situation into "stress release".*

*We also added new paragraphs (in "Introduction" and "Residual pressure affected by viscous/plastic flow" sections) to make clarification that in our case, we refer to viscous relaxation as a time-dependent process and plastic yield as time-independent process that limits the deviatoric stress in the host, thus also limits the residual inclusion pressure. Both of them are irreversible.*

Lines 48-50. Authors state that "Mechanical models show that both viscous creep (dislocation or diffusion creep of host) and plastic yield (radial or tangential micro-cracks) can cause significant

pressure relaxation (Dabrowski et al., 2015; Zhang, 1998).” While cited references indeed present viscous relaxation models, none of them presents mechanical model that shows plastic yield or radial and tangential microcracks. Care with references is needed.

*We agree that in Dabrowski et al. 2015, plastic yielding was not studied. But in Zhang 1998, he showed the effect of plastic yield on the stress distribution (Fig. 2B). Due to the limited differential stress in the host upon plastic yield, the stress state in the inclusion will be changed. In his section 4.3, Zhang (1998) focused on the radial cracks formed during decompression. Although he did not quantitatively show the amount of pressure release but he did mention about the fractures formed around various mineral inclusions depending on the bulk modulus of the inclusion and host.*

Section 2.1. Logic of this section can be improved. Equation (2) uses results of equation (4), which is further in the text. It is better to introduce plastic flow law (4) first and then give summary equation for total strain rate (2).

*This part is now clarified. We thank the reviewer for pointing it out.*

Lines 84 and 86. The choice of references for classical Tresca yield criterion and associated plastic flow law is a bit odd. There are much older, standard and very good textbooks that introduced those, e.g. [Hill, 1950; Kachanov, 1971].

*Reference is updated, we added Kachanov (1971) as suggested.*

Lines 85 – 89 and throughout the text. Parameter C in the Tresca yield condition is not cohesion. It is a half of the yield limit for simple tension of the host matrix in the case of spherical inclusions [Hill, 1950; Kachanov, 1971]. This is important to note because later in the text (in the discussion section) authors make estimations of this parameter based on the experimental data for cohesion and make conclusions for Raman-thermobarometry. Also, I would want to mention that Tresca criterion represents yielding due to dislocation sliding in crystalline materials at high pressures and thus cannot be taken as a proxy for fracturing. You need a more thorough discussion on the deformation mechanisms in the host rock to justify the choice of yield function and viscosity (Eq. 5). There are various deformation mechanism maps for viscosity can be found in the literature.

*This is a valid point and we agree with the reviewer. We have updated the reference based on the reviewer’s suggestion and carefully checked the entire manuscript to adjust “cohesion” into “yield strength”. We have also removed the parts for “fracturing” and replace them by plastic yield.*

Line 83. Wrong statement: “lambda is the plastic multiplier ($s^{-1}$) which guarantees that the plastic yield criterion is not exceeded”. Plastic multiplier provides the amount of the plastic deformation. However, in the numerical codes it is indeed calculated from yield criterion and consistency conditions.

*This sentence has been adjusted as suggested.*

Equation (9). Explain parameter delta.

*Clarified as suggested.*

Lines 102-105. Authors write that “This is done by choosing the following independent scales: the inclusion radius, temperature change, time, viscosity pre-factor of host, plastic cohesion of host, and the expected pressure perturbation that is given as follows” Again, be careful with your statements. These scales are not independent. You can have only one independent scale of pressure, time, temperature, length. Thus, viscosity factor and cohesion would be already dependent parameters.

*This is correct. We thank the reviewer for this point. We have corrected this sentence. The parameters we used to nondimensionalize the system are not independent, which has been noted in the revised manuscript by deleting “independent”.*

Line 109. It is not entirely clear why Pexp is chosen as a scale. Please explain this parameter, where it comes from.

*This is a good point. We missed the explanation for Pexp. It comes from the paper of Zhang (1998) which described the amount of residual pressure assuming constant bulk modulus and thermal expansivity. Using it as a pressure scale is advantageous as the inclusion pressure will vary from 0 to 1. Now this is clarified in the text.*

Also check Eq. 11. It is not logical to scale yield function F and cohesion to different scales.

*We thank the reviewer for this point. We have changed the scale for F with the yield strength of the host. This does not influence the other equations as F does not appear in other equations.*

Lines 123-127. Again, C is not cohesion. Please rewrite this para. Statements on the range of viscosity and yield limit must be supplemented with references and even better if with realistic numbers. I doubt that one can expect orders of magnitude variation in yield strength of minerals as it is stated by authors: “the cohesion of difference mineral may also vary by many several factors, potentially orders of magnitude”.

*We have removed all “cohesion” words following the suggestion. We have removed the statement of “several orders of magnitude”.*

Section 2.3. Given that there is no reference for the numerical approach, I assume itis original. Or was it previously reported somewhere? In general, there is a different level of detail in the paper. E.g. there is too much focus on standard non-dimensional analysis and almost nothing on non-trivial visco-elasto-plastic numerical scheme or on the elastic numerical solution for half-space in the following sections.

*We agree with the reviewer that the numerical approach is relatively short compared to other parts. We have added some new descriptions and references on this part. We would not say the numerical approach we presented as original, where we use finite difference method (staggered grid stencil) and iteratively solve for the three unknowns from three equations. The numerical stencil (staggered grid finite difference, mostly in 2D/3D) has been used widely (e.g. Gerya 2010, now cited in the text) and the iterative solver (Picard iteration) is also relatively common in numerical modelling.*

Section 2.4. It is hard to see the value of this section in the paper. Authors present analytical solution previously derived by Seo and Mura [1979]. However, no meaningful analysis or conclusions for the topic of the paper (i.e. Raman-thermobarometry) were derived from this solution. Its use for benchmarking of numerical code is also limited as analytical and numerical results are different due to various assumptions about material properties of inclusion. On the other hand, other analytical solutions used for benchmarking in section 2.3 are not resented at all. If authors choose to keep this solution, I would recommend discussing carefully boundary, initial conditions and its relation to the Raman-thermobarometry. For example, is it an incremental solution and does it show changes in stress from a specific initial condition? Or does it show stress distribution in an inclusion-host system without initial pre-stress? What do we learn from this solution?

*This is a very valid comment. A similar point has also been raised by the second reviewer. We have now reduced the focus of the "half-space" problem by moving all the derivations into appendix and we only left the final analytical formula for pressure distribution in the main text (which is a new result). We have added a new section discussing the application of the presented formula together with an updated figure (Fig. 3 in the revised version) to show the results of the analytical formula for pressure distribution of inclusion in half-space.*

*We agree that the application for numerical benchmark is limited by the fact that the presented formula is only applicable to homogeneous inclusion. However, due to the simplicity (compared to the analytical formulas of e.g Mindlin, and Seo & Mura) we argue that it is still useful. This we have discussed it in a new paragraph for a benchmarking purpose in the appendix.*

Line 172. Why Pexp is referred to as "initial residual pressure"? As this solution is presented now, there is no process in it, only static force equilibrium.

*Pexp is the initial overpressure that is already under force equilibrium in infinite host. As the inclusion approaches the thin-section surface, the inclusion pressure gets smaller than Pexp. This is now explained at the beginning of the new section of "Inclusion pressure modification due to proximity to thin-section surface".*

Section 3.1. Switch from one problem setup to another comes very abrupt here. Please document your simulation setup (geometry, boundary and initial conditions, properties of the host and inclusion) and state which problem you address (i.e. stress relaxation or sample preparation). The title of this section is inconsistent with the following sections.

*We have restructured the whole manuscript and clearly separate the results of the presented two models. Now this section directly continue from the visco-elasto-plastic 1D model so there should be no confusion on which model we refer to. We also added a short paragraph before it to clarify the simulation setup.*

Line 183. “This diagram may assist petrological investigations because De and C* can be evaluated based on experimental rock deformation data for different minerals...”Please discuss how De and C* can be evaluated based on experimental data. Which data is available?

*We have added new sentences in the following text to clarify it, e.g. using flow law to evaluate De and using microhardness test data to evaluate C*.*

Line 196. Awkward phrase: “...and De is located above the plastic onset...” Please reformulate.

*Done. We have changed it to De above one to describe the plastic dominant regime.*

Section 3.2. Describe problem setup, boundary and initial conditions. Given that you have two different problem setups in the paper it is confusing. Governing equations and a little bit info about numerical implementation would also fit here rather than supplementary materials in the same way as you present another model. Without such descriptions, it is hard to see the relevance to sample preparation problem. Do you consider just an equilibrium stress state, or do you have an incremental formulation that considers initial condition?

*This is a valid point. We have restructured the whole manuscript to split the two models. Also we have added new text here to elaborate the model setup. This we have clarified in new section 4.2 (place has been changed due to restructuring).*

Check for use of word “relaxation” here and rather use “release”. Check also for consistent use of “quartz-in-almandine” and “quartz-in-garnet” terms.

*This has been pointed out before by the reviewer and we completely agree. We have checked the word “relaxation” in the entire manuscript to carefully split it with “release” due to different rheology.*

Line 210-216. What are the implications for sample preparation, e.g. in terms of thickness etc?

*As this is the results part, we do not discuss any implications for sample preparation. But we did follow the reviewer’s suggestion by adding new text in Section 5.1 (Discussion) about sample preparation and inclusion picking procedure to avoid pressure release due to proximity to thin section surface.*

Line 223. “Assuming that the thin-section surface is sufficiently far away from a quartz inclusion and no microcracks appear around quartz inclusion...” I recommend replacing “microcracks” with “yield” as your solution does not consider microcracks and there is a discussion on microfracture later.

*Done.*

Line 227. “The flow law of garnet from Wang and Ji (1999) is applied”. Please describe briefly this law.

*This is a good point that we have previously missed. Now a new equation has been added for Wang and Ji’s flow law with numbers. (Eq. 21)*

Line 272. “The three mechanisms investigated here, i.e. viscous creep, plastic yield and proximity of inclusion...” Plastic yield was studied only together with creep, i.e. on a geological time scale. Plastic

yield without creep as might occur e.g. during sample preparation was not studied. Thus, I think it is more appropriate here to use term visco-plastic flow instead of plastic yield.

*Done. We thank the reviewer for pointing that out.*

Section 4.1. C is not cohesion, please check relevant values and your estimations for C.

*This point has been raised by the reviewer before and we agree. We have adjusted the terminology used here. We now refer C as the plastic yield strength. We have checked the entire manuscript to change cohesion into yield strength.*

Lines 283-289. "This suggests that plastic yield does not occur in an idealized scenario of isotropic, spherical quartz inclusion entrapped in infinite garnet host. However, such an ideal scenario is highly improbable in natural samples. The observed cracks in garnet host may be formed due to potential reasons including: 1) elevated differential stress when the inclusion is close to thin-section surface ("ring" shaped pattern in Fig.4a); 2) stress concentration at the corners of quartz inclusion (Whitney et al., 2000); 3) anisotropic elastic deformation of the quartz inclusion (e.g. Murri et al., 2018); 4) pre-fractures/weakness in garnet host before the entrapment of quartz inclusions."

While I agree with the possibility of elevated differential stress and stress concentrations at the corners, I would like to emphasize that this statement is based on the solution for materials obeying Tresca criterion, which does not describe fracturing. To make conclusions about fractures around inclusion, one needs to consider other failure criteria such as Griffith or Mohr-Coulomb, where cohesion and tensile strength play major role. Solutions for plasticity onset and failure pattern in elastoplastic and visco-plastic rocks with these failure criteria are available in the literature. They would give other estimations for pressure necessary to induce fractures.

*We agree with the reviewer on this point. Here, we have deleted the words related to cracks. The point is that we may still have localized stress due to the following reason stated above, hence localized dislocation around a non-spherical, anisotropic inclusion. Therefore, a statement on localized plastic yield around natural mineral inclusion is valid, just that we do not involve cracks in our discussion.*

Conclusions. "We presented a 1D visco-elasto-plastic model to study the inclusion-host system undergoing prograde/retrograde P-T path" There are at least two different models in this paper.

*We added "first" and "then" before the two sentences for the two models to separate them.*

"A simplified analytical solution for inclusion pressure (Eq. 32) close to stress-free thin-section surface is derived." The solution presented by authors was not new, it was re-derived after original paper by Seo and Mura [1979].

*We have rephrased this sentence so that it is clear that the solution was not original. The derivations were moved to the appendix.*

Please also make some statements on the implications for Raman-thermobarometry and how to use your results.

*This is a helpful comment. We have added some text in "Conclusions" about the petrological implications of our model and summarize what we have found about the determination of entrapment pressure of quartz inclusion and the application of garnet overstepping model.*

*In the end, we again thank the reviewer for all the detailed comments that greatly improved the quality and technical correctness of the manuscript.*

***General reply to reviewer 2***

*We thank the very positive feedback from the reviewer and helpful comments in the review letter. We have carefully considered all the comments given by the reviewer and made corresponding changes to the manuscript. In this reply letter, the original comments from the reviewer are in "*regular black*" and our replies are in "italic blue"*

I apologize for the delay of the review process but I had too many administrative issues to deal with first. The manuscript is actually one of those that make the review process very easy. It is well-written, it has well organized structure and the addresses a timely topic with a novel approach. On top what referee #1 has been already mentioned, I only have suggestions, basically no real criticism. I like the way the authors explain the methods in chapter 2. And finally discuss the most important findings of the study in a reasonable detail. I would only suggest to spent less words on the "distance to surface" issue (chapter 3.2) as this is not really new, but focusing more on the "over-" and "underestimation" of the pressure depending on the PT paths the samples take. This is really exciting and should be highlighted even more.

*We totally agree with the reviewer that the "distance to surface" issue has been studied in several papers cited in the manuscript. We took the advice and move the previous derivation part into the appendix. However, we would like to highlight that the new thing that we present is this very simple form of pressure distribution (now in Eq. 22). Compared to the cumbersome formulas of stress components in e.g. Seo and Mura (1979) and Mindlin and Cheng (1950), the pressure distribution can be simplified to a concise closed form. This is particularly relevant in studying the residual pressure distribution and pressure release due to proximity to thin-section surface. Also, when performing numerical model benchmark, this is particularly helpful because of its simplicity. If one wants to perform a fast validation on the numerical solution, our Eq. 22 can be easily used to compare with the pressure calculated with numerical code. Therefore, we leave the final equation for pressure distribution (Eq. 22) in the main text and most of the derivations in the appendix. The "distance to surface" part has been revised accordingly to clarify these points.*

To me the authors could consider to keep the inclusion-host relationship a bit broader in the

begin of the introduction, such as considering inclusions in a bit broader context (see Farber et al 2014 CMP, for instance), but this may result in a less sharp structure.

*We agree with the reviewer's point to make the text of wider appeal to general readers in petrology. Therefore, we have added several references including the suggested one at the beginning of the text to reach a broader audience.*